FLUID MODELING OF EXHAUST GAS DISPERSION FROM THE BOSTON EDISON VENTILATION SITE, CENTRAL ARTERY/THIRD HARBOR TUNNEL PROJECT

Prepared by

David E. Neff
Thomas Z. Tan
Robert N. Meroney

Final Report
(June 1988 - December 1988)

Fluid Mechanics and Wind Engineering Program
Department of Civil Engineering
Colorado State University
Fort Collins, Colorado 80523

Prepared for

Bechtel/Parsons Brinkerhoff
Central Artery/Third Harbor Tunnel Project
One South Boston
Boston, Mass. 02110

CSU Contract No. 2-97360

March 1989

CER88-89DEN-TZT-RNM-7

EXECUTIVE SUMMARY

Title:	Fluid Modeling of Exhaust Gas Dispersion from the Boston-Edison Ventilation Site, Central Artery/Third Harbor Tunnel Project
Contractors:	Civil Engineering Department Colorado State University Fort Collins, Colorado 80523
Principal Investigators:	D.E. Neff, T.Z. Tan and R.N. Meroney
Report Period:	July 1988 - December 1988

Objective: The Commonwealth of Massachusetts, in cooperation with the Department of Transportation, Federal Highway Administration, proposes to depress and widen the Central Artery through central Boston. The underground sections of the Central Artery and the Third Harbor Tunnel will be ventilated. Six to eight ventilation buildings are planned for the project. Two of the building sites, Parcel 7 and Boston Edison, are located in congested, heavily populated areas within the confines of downtown Boston. The complicated flow patterns associated with these sites clearly indicate the need for physical modeling of vent building air quality impacts. The Fluid Dynamics and Diffusion Laboratory at Colorado State University has conducted the wind tunnel physical modeling study requested by B/PB. The objectives of this model study were a) to provide visual information and concentration data on the environmental impact of several proposed vent building, stack height specifications, and b) summarize this information and data into a convenient format then discuss the advantages and disadvantages of the different vent building-stack specifications.

Results: Selection of the final building and exhaust stack configuration for the Boston-Edison Ventilator building will be based upon the consideration of its visual appearance within the Boston historic district, zoning regulations, and minimization of environmental impact. The environmental effects of exhaust from the ventilator stacks will depend upon tunnel traffic volume, ventilator flow rates, state and federal ambient air-quality regulations, building and plume aerodynamics, and local meteorology. This study evaluates through fluid modeling the influence of building and plume aerodynamics on plume dilution. Data is reported in terms of normalized concentrations (K coefficients) to permit concentration estimates for alternative traffic, exhaust and wind speed conditions. Concentrations can be estimated for alternative configurations, but acceptability must depend upon current air-quality standards.

ACKNOWLEDGEMENTS

The authors wish to express their gratitude to the staff and personnel of the Fluid Dynamics and Diffusion Laboratory at Colorado State University. Special thanks go to Mr. D. Parse and Mr. Q. Roberts who built both the Parcel 7 site model and the Boston-Edison site model. Appreciation is herewith presented to the Bechtel/Parsons Brinkerhoff (B/PB) selected by the Commonwealth of Massachusetts to manage the Central Artery and Third Harbor Tunnel Project.

TABLE OF CONTENTS

LIST OF TABLES

LIST OF FIGURES

LIST OF SYMBOLS

A,B,C	Constants
BR	Blockage ratio
C_p	Specific heat capacity at constant pressure
E	Hot wire voltage output
h	Height of the obstacle
g	Gravitational acceleration
k	Roughness length
L	Length
Q	Flow rate
S	Distance downstream of the obstacle
T	Temperature
U	Wind velocity
u_*	Friction velocity
X	Concentration
x	Distance
Z	Height above ground
z_o	Roughness length

Greek Characters

$\dot{\rho}$	Air density
Γ	Abiabatic potential temperature lapse rate
κ	Thermal conductivity
μ	Dynamic viscosity
ν	Kinematic viscosity
ρ	Density
χ	Fraction of a gas component
Ω	Angular velocity of earth - $0.726*10^{-4}$ rad/s

Dimensionless Parameters

Ec	Eckert number
Ma	Mach number
Re	Reynolds number
Ri	Bulk Richardson number
Ro	Rossby number
Pr	Prandtl number
V	Volume flux ratio $(Q/U_H L^2)$

1. INTRODUCTION

The Commonwealth of Massachusetts, in cooperation with the Department of Transportation, Federal Highway Administration, proposes to depress and widen the Central Artery through central Boston. The Bechtel/Parsons Brinkerhoff (B/PB) joint venture has been selected by the Commonwealth of Massachusetts to manage the Central Artery and Third Harbor Tunnel Project. The work performed by B/PB is under the direction of the Massachusetts Department of Public Works (MADPW).

The underground sections of the Central Artery and the Third Harbor Tunnel will be ventilated. Seven ventilation buildings are planned for the project. Two of the building sites, Parcel 7 and Boston Edison, are located in congested, heavily populated areas within the confines of downtown Boston. The complicated flow patterns associated with these sites clearly indicate the need for physical modeling of vent building air quality impacts.

The Fluid Dynamics and Diffusion Laboratory at Colorado State University has conducted the wind tunnel physical modeling study requested by B/PB. The objectives of this model study are:

1. To provide visual information and concentration data on the environmental impact of several proposed vent building, stack height specifications, and
2. Summarize this information and data into a convenient format then discuss the advantages and disadvantages of the different vent building-stack specifications.

These objectives will be separately carried out for a Phase 1 series of tests oriented on the Parcel 7 building region and a Phase 2 series of tests oriented on the Boston Edison building region. This report deals only with the Phase 2 study.

Section 2.0 discusses the physics of modeling plumes at reduced length scales. Section 3.0 describes the data acquisition techniques used to perform this study. Section 4.0 lists the test program results. Section 5.0 is a discussion of selected data.

2. MODELING OF PLUME DISPERSION FROM TUNNEL VENTILATOR SITES

The Appendix describes in general terms the scaling laws that cover a large class of fluid modeling applications. The intent of this section is to specifically address the modeling techniques used in the present study.

The exhaust air released from the tunnel ventilators will exit at ambient temperatures and densities; hence, the source gas used in the model was primarily nitrogen released at room temperatures (specific gravity ≈ 1.0). Thus the plume mass flux, momentum flux and volume flux are essentially equivalent ratios, and the plume Froude number is not a relevant parameter.

The wind approaches the Boston city center over either suburban roughness or the harbor sea surface. The Boston-Edison site is located between downtown Boston and the Boston Inlet Harbor. Replicas (at reduced scale of 1:384) of all buildings within 2,300 feet of the Boston-Edison vent building were constructed and placed on the downwind turntable in the wind tunnel. The wind characteristics approaching the Boston-Edison site, for all wind directions excluding the NE to SE sector, were simulated with a generic suburban roughness constructed from one-inch cubes. The upwind fetch approaching the Boston-Edison site, for winds out of the NE to SE sector, is predominately over the harbor or the lower buildings in east Boston. Thus, for the wind tunnel simulations of these wind directions the upwind generic roughness was removed.

The modeling parameter decision process yielded the following conclusions:

1. Maximum field dispersion distance of interest and size of the FDDL Environmental Wind Tunnel facility resulted in the selection of a 1:384 model length scale ratio.

2. Neutral stratification in the laboratory was used to reproduce the dispersion dynamics of the windy Boston area.

3. Wind-tunnel floor roughness was adjusted to produce properly scaled wind shear and turbulent structure.

4. Model wind speed and stack exit velocity were set at large enough magnitudes to assure Reynolds number independence of approach flow and stack flow.

5. Model wind velocity to plume velocity ratios were set equal to the field values; thus assuring similarity of plume trajectories.

3. DATA ACQUISITION AND ANALYSIS TECHNIQUES

Laboratory measurement techniques are discussed in this section, along with conversion methods used to convert measured model quantities to their meaningful field equivalents. Some of the methods used are conventional and need little elaboration.

3.1. WIND-TUNNEL FACILITIES

The experiments were performed in the Environmental Wind Tunnel (EWT) shown in Figure 1. This wind tunnel, especially designed to study atmospheric flow phenomena, incorporates special features such as an adjustable ceiling, a rotating turntable and a long test section to permit adequate reproduction of micrometeorological behavior. Mean wind speeds of 0.1 to 15 m/sec in the EWT can be obtained. Boundary-layer thickness up to 1.2 m can be developed "naturally" over the downstream 6 m of the EWT test section by using vortex generators at the test section entrance and surface roughness on the floor. The flexible test section on the EWT roof is adjustable in height to permit the longitudinal pressure gradient to be set at zero.

3.2. WIND PROFILE MEASUREMENTS

Velocity measurements were made with single-hot-film probes and anemometry equipment manufactured by Thermo-System, Inc. (TSI).

Velocity Standard

The velocity standard used in the present study consisted of a Matheson Model 8116-0154 mass flowmeter and a profile conditioning section designed and calibrated by the Fluid Dynamics and Diffusion (FDDL) staff at Colorado State Universty (CSU). The mass flowmeter measures mass flow rate independent of temperature and pressure. The profile conditioning section forms a flat velocity profile of very low turbulence at the position where the hot-film-probe is located. Incorporating a measurement of the ambient atmospheric pressure, temperature and a profile correction factor permits the calibration of velocity at the measurement station from 0.15-2.2 m/s to within ± 5 percent.

Single-Hot-Film Probe Measurements

Single-hot-film (TSI 1210 Sensor) measurements were used to document the longitudinal turbulence levels for the approach flow conditions. During calibration the probe voltages were recorded at several velocities covering the range of interest. These voltage-velocity (E,U) pairs were then regressed to the equation $E^2 = A + BU^c$ via a least squares approach for various assumed values of the exponent c. Convergence to the minimum residual error was accelerated by using the secant method to find the best new estimate for the exponent c.

The hot-flim-probe was mounted on a vertical traverse and postioned over the measurement location in the wind tunnel. The anemometer's output voltage was digitized and stored within an IBM AT computer. This voltage time series was converted to a velocity time series using the inverse of the calibration equation; $U = [(E^2 - A)/B]^{1/c}$. The velocity time series was then analyzed for pertinent statistical quantities, such as mean velocity and root-mean-square turbulent velocity fluctuations. The computer system would move the velocity probe to a vertical position, acquire the data, then move on to the next vertical postions, thus obtaining an entire vertical velocity profile automatically.

Error Statement

The calibration curve yielded hot film anemometer velocities that were always within 2 percent of the known calibrator velocity. Considering the accumulative effect of calibrator, calibration curve fit and other errors the model velocity time series should be accurate to within 10 percent.

3.3. FLOW VISUALIZATION TECHNIQUES

A visible plume was produced by passing the metered simulant gas through a smoke generator (Fog/Smoke Machine manufactured by Roscolab, Ltd.) and then out of the modeled stack. The visible plumes for each test were recorded on VHS video cassettes with a Panasonic Omnivision II camera/recorder system. Run number titles were placed on the video cassette with a title generator.

3.4. CONCENTRATION MEASUREMENTS

The experimental measurements of concentration were performed using a Hewlett Packard gas-chromatograph and sampling systems designed by Fluid Dynamics and Diffusion Laboratory staff.

3.4.1. *Gas Chromatograph*

A gas chromatograph (Hewlett-Packard Model 5710A) (GC) with flame ionization detector (FID) operates on the principle that the electrical conductivity of a gas is directly proportional to the concentration of charged particles within the gas. The ions in this case are formed by the burning a mixture of hydrogen and the sample gas in the FID. The ions and electrons formed pass between an electrode gap and decrease the gap resistance. The resulting voltage drop is amplified by an electrometer and passed to a Hewlett-Packard Model 3390A integrator. When no effluent gas is flowing, a carrier gas (nitrogen) flows through the FID. Due to certain impurities in the carrier, some ions and electrons are formed creating a background voltage or zero shift. When the effluent gas enters the FID, the voltage increase above this zero shift is proportional to the degree of ionization or correspondingly the amount of tracer gas present. Since the chromatograph used in this study features a temperature control on the flame and electrometer, there is very low drift of the zero shift. Even given any zero drift, the HP 3390A, which integrates the effluent peak, also subtracts out the zero drift.

The lower limit of measurement is imposed by the instrument sensitivity and the background concentration of tracer within the air in the wind tunnel. Background concentrations were measured and subtracted from all data quoted herein.

3.4.2. *Sampling System*

The tracer gas sampling system consists of a series of fifty 30 cc syringes mounted between two circular aluminum plates. A variable-speed motor raises a third plate, which lifts the plunger on all 50 syringes, simultaneously. Computer controlled valves and tubing are connected such that airflow from each tunnel sampling point passes over the top of each designated syringe. When the syringe plunger is raised, a sample from the tunnel is drawn into the syringe container. The sampling procedure consists of flushing (taking and expending a sample) the syringe three times after which the test sample is taken. The draw rate is variable and generally set to be approximately 6 cc/min.

The sampling system was periodically calibrated to insure proper function of each of the valves and tubing assemblies. To calibrate the sampler each intake was connected to a manifold. The manifold, in turn, was connected to a gas cylinder having a known concentration of tracer gas. The gas was turned on, and a valve on the manifold was opened to release the pressure produced in the manifold. The manifold was allowed to flush for about one minute. Normal sampling procedures were carried out during calibration to insure exactly the same procedure is reproduced as when taking a sample from the tunnel. Each sample was then analyzed for tracer gas concentration. Percent error was calculated, and "bad" syringe/tube systems (error > 2 percent) were not used or repaired.

3.4.3. *Test Procedure*

The test procedure consisted of:

1) Setting the proper tunnel wind speed,
2) Releasing the metered mixtures of source gas from the plant stack,
3) Withdrawing samples of air from the tunnel designated locations, and
4) Analyzing the samples with a FID.

The samples were drawn into each syringe over a 200 s (approximate) time period and then consecutively injected into the GC.

The procedure for analyzing the samples from the tunnel is:

1) Introduce the sample into the GC which separates the ethane tracer gas from other hydrocarbons,
2) The voltage output from the chromatograph FID electrometer is sent to the HP 3390A Integrator,
3) the HP 3390A communicates the measured concentration in ppm to an IBM computer for storage, and

4) These values, χ_{mea}, along with the response levels for the background χ_{bg} and source χ_{source} are converted into source normalized model concentration by the equation:

$$\chi_m = \frac{\chi_{mea} - \chi_{bg}}{\chi_{source} - \chi_{bg}}$$

5) Field equivalent concentration values are related to model values by the equation:

$$\chi_p = \frac{\chi_m}{\chi_m + (1-\chi_m)[(\frac{T_a}{T_s})V]_m/[(\frac{T_a}{T_s})V]_p}, \quad \text{where } V = Q/U_H L^2,$$

and L is the characteristic length scale. When there is no distortion in the model-field volume flux ratio, V, and the plumes are isothermal this equation reduces to $\chi_p = \chi_m$.

Error Statement

Finite background concentrations, χ_{bg}, resulted from previous tests within the laboratory, these low levels could be measured to accuracies of 20 percent. The larger measured concentrations, χ_{mea}, were accurate to 2 percent. The source gas concentration, χ_{source}, was known to within 10 percent. Thus the source normalized concentration for $\chi_{mea} >> \chi_{bg}$ was accurate to approximately 10 percent. For low concentration values, $\chi_{mea} > \chi_{bg}$, the errors are larger.

4. TEST PROGRAM AND DATA FOR BOSTON-EDISON (PHASE 2)

A physical modeling study of the Boston-Edison site vent buildings was performed to assist in predicting environmental impacts for several proposed stack-building configurations. This involved:

1) The 1:384 reduced scale construction of the different potential Boston-Edison stack-building configurations along with the all buildings within 2300 feet of Boston-Edison site,
2) The placement of this model into a wind tunnel facility with the appropriate upwind roughness for this site,
3) Acquisition of velocity and turbulence profiles approaching and at the modeled Boston-Edison site for each wind direction of interest,
4) Video taping of the model plume for 31 different combinations of stack-building height and type, wind direction and stack exit velocities,
5) Concentration measurements at 45 different sampling locations for 134 different combinations of stack-building height and type, wind direction and stack exit velocities, and
6) The presentation of a final report that lists all data and discusses all experimental techniques used to acquire this data.

The following sub-sections discuss these topics in greater detail.

4.1. MODEL CONSTRUCTION

Based on atmospheric data over the Boston area, the size of the concentration grid, and modeling constraints discussed in Section 2 and the Appendix, a model scale of 1:384 was selected. Since the Environmental Wind Tunnel (see Figure 1) had a 12 foot turntable this allowed for the reduced scale construction of all significant buildings within a 2300 foot radius of the Boston-Edison vent building site. The location of the Boston-Edison site along with a circle demarking the portion of downtown Boston which was replicated is shown in Figure 2.

The buildings surrounding the vent structures were fabricated from styrafoam and were placed in their appropriate locations on a 12 foot diameter 1/4 inch masonite sheet. All roads and waterways were painted on this masonite sheet. The topography changes were modeled by layering the appropriate number of 1/4 inch sheets to match the land contours within the modeled area. Figure 3 is a picture of the entire 12 foot turntable model. The terrain upwind of the turntable area was modeled with either a smooth surface or a generic one inch roughness (field equivalent height of 32 feet), dependent on whether the winds were approaching over the harbor surface or not.

Four different ventilator buildings were constructed. The primary ventilator building, the Boston-Edison unit, had two different building designs, one designated as 2A the other as 2B. The Boston-Edison unit was located at the center of the 12 foot turntable model. The other three ventilator buildings were located at sites along the harbor shore adjacent to the Boston-Edison site. These were designated as the J. Hook, the Atlantic and the Appraiser vent buildings. Figure 4 through Figure 9 show pictures of these different vent buildings. The stacks on each of the four ventilator buildings were adjustable in height of 240 or 300 feet. The different buildings were construted of masonite, whereas the stacks were fabricated from tack board. Each building contained a manifold through which metered simulate gases were directed to the stacks. Each ventilator building used 14 vent fans to blow exhaust gases through 10 by 14 foot (inside measure) openings. These individual stacks were arranged into a different patterns for each of the vent buildings.

4.2. VELOCITY PROFILES

The techniques employed in the acquisition of velocity profiles are discussed in Section 3.2. The site model was located on a turntable, thus it could be rotated to simulate the different wind directions. An approach flow upwind of the turntable model, typical of a suburban environment, was created through the placement of vortex generators at the tunnel entrance followed by 30 feet of 1 inch cube roughness on the tunnel floor. An approach flow upwind of the turntable model, typical of a harbor-ocean environment, was created by removing 10 feet of the one inch cube roughness just upwind of the turntable.

Table 1 summarizes the conditions for all the velocity profiles obtained in this study. Table 2 through Table 4 present the data for each of these profiles. Figure 10 through Figure 17 display plots of these mean velocity and longitudinal turbulent intensity profiles. The height coordinate in these tables and figures has been normalized by a model reference height of 1 meter (equivalent field height of 1260 feet); thus, to obtain actual field heights multiply the normalized value by 1260. The velocity coordinate in these tables and figures has been normalized by the model velocity at 1 meter height. The model reference velocities used for each of the profiles are listed in Table 1. Since a neutral boundary layer's velocity is invariant with respect to wind speed the normalized profiles presented can be converted to any field velocity at a specific height by the appropriate multiplicative constant.

The crosswind uniformity of the flow approaching the model site inside the wind tunnel was established in the Phase I study, Neff et.al. (1988) (cite Pg.31) for the Parcel 7 ventilator site.

The first four profiles (numbers 1, 2, 3 and 4) tested the invariance of the mean and turbulent velocity profiles with respect to different wind tunnel reference wind speeds. The data for these profiles are tablulated in Table 2. The mean velocity profiles for an upwind fetch typical of a suburban environment are shown in Figure 10 and the turbulent intensity profiles are shown in Figure 11. The mean velocity profiles for an upwind fetch typical of a harbor-ocean environment are shown in Figure 12 and the turbulent intensity profiles are shown in Figure 13. These figures and table show that the wind tunnel approach flow was indeed invariant with respect to wind speed.

The approach mean velocity profiles for a suburban roughness condition (numbers 1 and 2) were regressed to find the best log-log and log-linear fit. The log-log regression produced a power law exponent, p, equal to 0.24; i.e. $U/U_r = (z/z_r)^p$. The log-linear regression ($U/u_* = 2.5\ln\{(z-d)/z_o\}$) found a best fit roughness length, z_o, of 0.9 meters (field scale) and a displacement thickness, d, of 4.8 meters. These values of the power law exponent and the roughness length are appropiate for a suburban roughness condition. The approach mean velocity profiles for a harbor-ocean roughness condition (numbers 3 and 4) were also regressed to find the best log-log and log-linear fit. The log-log regression produced a power law exponent, p, equal to 0.17. The log-linear regression found a best fit roughness length, z_o, of 0.2 meters (field scale) and a displacement thickness, d, of 0.0 meters. These values of the power law exponent and the roughness length are appropiate for a harbor-ocean roughness condition.

The next eight profiles (numbers 5 through 12) were obtained over the center of the model at the Boston-Edison ventilator site. Each profile was for a primary wind directions from 0° to 360° at 45° increments. The wind direction and roughness condition for each of these profiles is listed in Table 1. The profile data for wind directions 0° through 135° are tablulated in Table 3. The mean velocity profiles are shown in Figure 14 and the turbulent intensity profiles are shown in Figure 15. The profile data for wind directions 180° through 315° are tablulated in Table 4. The mean velocity profiles are shown in Figure 16 and the turbulent intensity profiles are shown in Figure 17. These two sets of figures show the influence of upwind structures on the local velocities over the Boston-Edison site. The most radical influence of upwind structures on the wind is seen in profile number 5 where the wind direction was from north (N).

4.3. VISUALIZATION TEST RESULTS

Techniques employed to obtain a visible plume are discussed in Section 3.3. Table 5 show the test conditions for 31 flow visualization tests over the Boston-Edison building region. The four different vent buildings at their proper site locations were investigated for two different stack exhaust flow rates and a variety of wind directions. The wind velocity for all these tests was 5 m/s at 30 meters height approaching the modeled area. The wind velocity at a certain height above the Boston-Edison site for a specific wind direction may be calculated by the following procedure:

1) The approach flow velocity profiles taken just upwind of the turntable model area indicate that when a 5 m/s (16.4 ft/s) velocity exists at a 30 meter height then the velocity at 384 meters is 5*(1/0.485) = 10.4 m/s (the normalized velocity on Profiles 1 and 2 at height 0.078 is roughly 0.485) for suburban roughness and is 5*(1/0.620) = 8.06 m/s (on Profiles 3 and 4) for harbor-ocean roughness, and

2) Multipling the normalized velocity values in the profile of interest (see section 4.2 above) by 10.4 m/s (34.1 ft/s) or 8.06 m/s (26.4 ft/s), depending on the appropriate approach flow condition will yield the velocity at the desired height.

Table 6 lists for each of the 31 visual test observations on stack downwash, building downwash, cavity mixing, plume descent, plume lofting, skyscraper impingement and other pertinent comments. Documentation on video cassettes of all visual tests have been provided to the sponsor prior to this report. Given a field to model wind speed ratio of 10 (= [5 m/s]/[0.5 m/s]) and a model to field length scale ratio of 384, then the time scale ratio between the model and the field is 1:38.4. Thus phenomena observed over the model in the wind tunnel will occur 38.4 times faster than observed at full scale. If the TV tapes were replayed in slow motion (38.4 times slower than the recorded speed), the observed plume trajectories and motions would appear realistic.

4.4. CONCENTRATION DATA RESULTS

Techniques employed to obtain the concentration data are discussed in Section 3.4. Table 7 describes the 45 sampling locations and provides the associated building code number, building description and distances from model center. Figure 18 shows all the concentration sampling locations marked on a map of the modeled area. Figure 19 shows a schematic of the manner simulant stack gases were introduced into the wind tunnel and subsequently sampled for concentration analysis. Table 8 and Table 9 summarize the concentration test conditions for all 134 runs performed. The field and model wind speeds indicated in this table were at heights of 30 meters and 7.9 cm, respectively. The conversion from these upwind velocity values to local values above the Boston-Edison site is the same as that described previously in Section 4.3 above.

Table 10 to Table 18 present the normalized concentration data, $(\chi U_H/Q)*10^9$, for all tests. This normalized concentration has units of ft^{-2}. This normalized format is convenient because the concentration results, χ, from a test at one particular combination of wind speed, U_H, and flow rate, Q, can be extrapolated to other U_H, Q values provided that the ratio, U_H/Q, remains the same. Note that U_H is the wind speed at 30 meters height approaching the model area and not the value of wind speed above the vent site. The total flow rate, Q, out of the stacks is the exit velocity for a particular run times the total stack exit area. The stack exit velocities for each run are listed in Table 8. The total exit area for all the vent building stacks was always 1960 ft^2.

5. DISCUSSION AND RECOMMENDATIONS

Selection of the final building and exhaust stack configuration for the Boston-Edison site will be based upon the consideration of its visual appearance within the Boston historic district, zoning regulations, and minimization of environmental impact. The environmental effects of exhaust from the ventilator stacks will depend upon tunnel traffic volume, ventilator flow rates, state and federal ambient air-quality regulations, building and plume aerodynamics, and local meteorology. This study evaluates through fluid modeling the influence of building and plume aerodynamics on plume dilution. Data is reported in terms of normalized concentrations, K, where

$$K = \chi U/Q,$$

to permit concentration estimates for alternative traffic, exhaust and wind speed conditions. Concentrations can be estimated for alternative configurations, but acceptability must depend upon current air-quality standards.

The following discussion will focus upon evidence for reliability and consistency within the data set and advantages or disadvantages of different building and stack configurations.

5.1. SMOKE VISUALIZATION RESULTS

As noted in Section 4.3 a total of 31 smoke test cases were performed to evaluate the relative dispersion that occurs for various vent stack heights, exit flow velocities and site orientations. Tests were grouped to examine the relative effects of stack height, exit flow velocity, adjacent garage height, and site orientation. Table 6 summarizes observations of plume behavior for each visualization run. The observations note the presence or absence of

i) Stack downwash - plume flagging or suction of smoke into stack wake

ii) Building downwash - suction of plume downward into building cavity

iii) Cavity mixing - mixing of plume throughout downwind building cavity

iv) Plume descent - deflection of plume groundward over building cavity

v) Plume lofting - plume little influenced by building, plume remains aloft.

vi) Skyscraper impingement - Elevated plume stagnates against faces of downwind tall buildings

To select a most favorable site, the four potential vent building sites were judged on the following factors:

a) Severity of downwash effects - When air encounters an obstruction, a disturbed flow region results in the lee of the obstruction. The height and width of this region is dependent on the shape of the obstacle. If a plume is released at a height near this region, the plume can become entrained (downwash or cavity mixing) into the region and cause significantly higher concentrations close to the source. The smoke tests were used to judge whether or not the plume was entrained in the lee of the potential vent building and/or the nearby tall structures for various wind directions. The smoke tests also allowed the relative intensity of this entrainment to be judged between sites.

b) Plume impaction on sensitive areas - All four potential vent buildings were evaluated for direct plume impaction on sensitive areas. These areas, selected as being obvious points of human congregation, are: the boston Harbor Hotel, the Rowe's Wharf and Harbor Towers area, One Financial Plaza Building and South Station area, and the Boston Children's Museum and Victoria Station Restaurant area. Plume impaction on other nearby tall structures was assumed to be unavoidable between sites and was later analyzed quantitatively in the concentration tests.

c) Other effects - Any unusual flow effects for the four possible vent building sites that have the potential to cause large variations in pollutant concentrations were noted. These unusual flow effects are caused mostly by wind channelling between buildings for a particular wind direction.

The cases studied may be categorized and grouped to reveal data trends. Examination of the visual records of these experiments reveals:

a) Exit Flow Velocity (ft/min): 800, 1600.

The vent gases are expected to exhaust at near ambient temperatures; hence, the vent plume will have little or no thermal buoyancy. Thus, plume rise will occur only as a result of vertical momentum. Higher exit flow velocities will add effective height to the vent stack. In addition low exhaust velocities ($W/U < 1.5$) may permit local downwash behind the vent stack, reducing the effective stack height significantly. Tests show that the 800 ft/min exhaust velocity permits significant downwash of the plume down the side of the stack directly into the building cavity. A 1600 ft/min exhaust velocity in a 5 m/sec wind field ($W/U = 1.6$) minimizes local building downwash effects.

b) Vent Site:

Boston Edison Substation:

For most wind directions studied, plume entrainment in the vent building cavity and nearby building cavities was observed when the exit flow rate was 900 fpm. At 1600 fpm plume entrainment was minimized. The plume was observed to have direct impact on the Rowe's Wharf-Harbor Towers area, the Boston Harbor Hotel, and the Children's Museum. With a northwest wind the upwind buildings produced a noticeable flow blocking effect causing the plume to rise higher than normal and impact further downwind from the Childres's Museum.

470 Atlantic Avenue:

This site exhibited many of the same findings as the boston Edison Substation site except that the plume entrainment was more severe. Additionally, the plume also had direct impact on the South Station-One financial Plaza area.

J. Hook Co.:

At the lower exit flow velocity (800 fpm) some plume entrainment was observed in the lee of the vent building. However, at 1600 fpm this effect was minimized and slight entrainment was observed in the lee of nearby buildings. With a northwest wind the upwind buildings caused a noticeable flow blocking effect such that the wind speed in the region behind these buildings was lower than the oncoming undisturbed flow. Consequently, the plume rose to a greater than normal height and touched down well beyond the Children's Museum. With an east-northeast wind, the plume was channeled paralled to Atlantic Avenue and caused a direct impact on One Financial Plaza. The plume generally missed the Rowe's Wharf-Boston Harbor Hotel area.

Appraiser's Building:

For most wind directions only slight plume entrainment was noticed in the lee of the vent building. However, the plume became entrained in the lee of buildings to the south. Except for the low exit flow velocity (800 fpm) case, this site generally exhibited the least amount of direct plume impaction on the Rowe's Wharf-Boston Harbor Hotel area. Similarly to what was observed for the J. Hook Co. site, the plume became channeled parallel to Atlantic Avenue with an ENE wind and caused a direct impact on the South Station-One Financial Plaza area.

c) Site Orientation: NNE, NE, ENE, E, ESE, SE,
SSE, S, SSW, NW, NNW.

The model was rotated to allow approach winds from the 16 major compass points. As the flow interacted with upwind buildings and the shape of the vent building the plume trajectory was modified by the variation in streamline patterns.

Several patterns reoccurred no matter the building configuration examined. Winds over the Boston downtown from the W through N directions were blocked by the tall buildings, which produced a sheltered low-wind region at the Boston-Edison site. Plumes exhausting into this wind environment were lofted quite high by their initial momentum; hence, they rarely penetrated the local wake region, and the plume touched down farther downwind.

Winds from the SE direction passed over only low rise residential areas before reaching the Boston-Edison site. High wind speeds at stack height deflected the plume immediately; hence, downwash was often significant. Furthermore, even plumes which did not reach ground level quickly often impacted the tall skyscrapers which stand to the NW. Such conditions will result in maximum concentrations at elevated samplers located on roof tops.

Conclusions from Smoke Visualization Tests:

The visualization tests provided observations which provided focus for the concentration experiments. The major conclusions were:

1. Vent exit velocities which exceeded 1.5 times the reference wind speed reduced building downwash. Consequently exit velocity 1600 ft/min was more desireable than the 800 ft/min flow velocity.

2. The smoke tests were first conducted with a vent building stack 240 feet high. This stack height exceeds the cavity height (234 ft) of the vent building which is 156 ft such that cavity effects can be minimized. During the smoke tests it was observed that a higher stack height could potentially mitigate some of the observed effects. Based on this observation a higher stack height of 300 feet was used in the concentration tests to determine, quantitatively, differences between these cases.

3. Among all sites, smoke visualization of direct plume impact varied widely with no clear choice between sites. Neither site could be conclusively selected as the best of the four sites. However, the Boston Edison Substation and J. Hook Company sites generally had less incidence of plume entrainment and direct plume imnpact on sensitive receptors than the other two sites.

4. The SE wind directions were identified as critical directions having the potential for high concentrations.

5.2. VERIFICATION OF FLUID MODEL RELIABILITY

Similarity of flow and dispersion of gas plumes over the Boston city complex must exist to obtain reliable estimates of concentrations. Appendix Section A.2.1 notes that equivalence is generally assured if the characteristic Reynolds number (or model velocity) is sufficiently large. Tests were performed during the Phase I study (cite Pg.31) over the Parcel 7 ventilator site (concentration test runs 15 through 19, in Neff, et.al.(1988)) to determine the minimum tunnel wind speed at which the K coefficients did not vary. Although runs were performed over a five-fold range in magnitude of wind speeds and ventilator flow rates, the ratio of exhaust velocity to wind speed was held constant at 0.81. Thus, sample point concentrations in terms of ppm or K coefficient should remain constant if similarity holds. In the Phase I study (cite Pg.31) displays the Reynolds number independence results. All values for prototype reference wind speeds greater than 5 m/s were equivalent; whereas the values were less for a prototype wind speed of 2.5 m/s. Since Reynolds number independence holds for wind speeds at 5 m/s and greater, all concentration and visualization test runs for both the Parcel 7 and Boston-Edison sites were performed at prototype wind speeds of 5 m/s.

5.3. INFLUENCE OF ALTERNATIVE STACK CONFIGURATIONS UPON CONCENTRATIONS

Given no other controlling factors (such as zoning regulations or cost) it is evident minimum surface concentrations will occur for maximum stack height, minimum building height, and maximum exhaust velocity. Figure 20 compares sampler concentrations for the SE wind direction for stack heights of 240 and 300 feet. The taller stack generally produce smaller sampler concentrations.

Greater improvement in sample point concentrations can be obtained by increasing stack velocity. Figure 21 compares sampler concentrations for the SE wind direction for exhaust velocities varying from 400 to 3200 fpm. A four-fold increase in stack velocity produces about a ten-fold decrease in concentration, whereas an eight-fold increase in stack velocity produces about a twenty-fold decrease in concentration. Stack downwash may occur for exhaust velocity to wind speed ratios less than 1.5. For the Boston-Edison complex a 5 m/sec wind speed the 400 and 800 fpm conditions permit significant stack downwash ($W/U < 1$); whereas, downwash is usually absent at large exhaust velocities ($W/U > 1.6$).

Wind direction combines with building orientation, building and stack downwash, exhaust velocity and sample location to produce a wide variance in sample concentrations. Figure 22, Figure 23 and Figure 24 consider sample location concentration variation for a 300 foot stack exhausting at 1600 fpm in a 5 m/sec wind. As expected most samples only show finite concentrations when the wind trajectory is from the ventilator building toward the sample location. Maximum K concentrations lie beween 4 to 5 x 10^{-6}. These concentrations can occur for winds from the ENE, ESE, SE and SSW. Maximum concentrations occur at elevated sample locations as a result of plume impingement on tall buildings.

5.4. INFLUENCE OF SITE LOCATION UPON CONCENTRATIONS

Two ventilation sites were selected according to the smoke visualization tests, the Boston Edison Substation and the J. Hook Co., for the intermediate concentration measurements. The intermediate concentration measurements were made for releases from each of the two stack heights (240 and 300 feet) at two exit flow velocities (400 and 1600 fpm) for each site. The 1600 fpm case was the design base case and the

400 fpm case was for plume downwash studies. Three wind directions (NE, ENE, SSW) were studied for each site at the specified exit flow velocity. This was done to study the impact resulting from each of these sites on One Financial Plaza, the Federal Reserve Building and Rowe's Wharf area.

Based on the results of the intermediate concentration tests, it was evident that releases from the J. Hook site resulted in higher concentration at most of the studied areas than releases from the Boston Edison site. Therefore, the Boston Edison site was selected as the proposed vent building location.

APPENDIX: MODELING OF PLUME DISPERSION

To obtain a predictive model for a specific plume dispersion problem, one must quantify the pertinent physical variables and parameters into a logical expression that determines their inter-relationships. This task is achieved implicitly for processes occurring in the atmospheric boundary layer by the formulation of the equations of conservation of mass, momentum and energy. These equations with site and source conditions and associated constitutive relations are highly descriptive of the actual physical interrelationship of the various independent variables (space and time) and dependent variables (velocity, temperature, pressure, density, concentration, etc.).

These generalized conservation statements subject to the typical boundary conditions of atmospheric flow are too complex to be solved by present analytical or numerical techniques. It is also unlikely that one could create a physical model for which exact similarity exists for all the dependent variables over all the scales of motion present in the atmosphere. Thus, one must resort to various degrees of approximation to obtain a predictive model. At present, purely analytical or numerical solutions of boundary layer, wake, and plume dispersion are unavailable because of the classical problem of turbulent closure (Hinze, 1975). However, boundary layer wind tunnels are capable of physically modeling plume processes in the atmosphere under certain restrictions. These restrictions are discussed in the next sections.

A.1 FLUID MODELING OF THE ATMOSPHERIC BOUNDARY LAYER

The atmospheric boundary layer is that portion of the atmosphere extending from ground level to a height of approximately 1000 meters within which the major exchanges of mass, momentum, and heat occur. This region of the atmosphere is described mathematically by statements of conservation of mass, momentum and energy (Cermak, 1975). The mathematical requirements for rigid laboratory/atmospheric-flow similarity may be obtained by fractional analysis of these governing equations (Kline, 1965). This methodology scales the pertinent dependent and independent variables by size and then casts the equations into dimensionless form by dividing by one of the coefficients (the inertial terms in this case). Performing these operations on such dimensional equations yields dimensionless parameters commonly known as:

Reynolds number	$Re = (UL/\nu)_r$	=	$\dfrac{\text{Inertial Force}}{\text{Viscous Force}}$
Bulk Richardson number	$Ri = [(Lg\Delta T/T)/U^2]_r$	=	$\dfrac{\text{Gravitational Force}}{\text{Inertial Force}}$
Rossby number	$Ro = (U/L\Omega)_r$	=	$\dfrac{\text{Inertial Force}}{\text{Coriolis Force}}$

Prandtl number $\quad Pr = [\nu/(k/\rho C_p)]_r \quad = \quad \dfrac{\text{Viscous Diffusivity}}{\text{Thermal Diffusivity}}$

Eckert number $\quad Ec = [U^2/C_p\Delta T]_r$

A.1.1 Exact Similiarity

For exact similarity between flows which are described by the same set of equations, each of these dimensionless parameters must be equal for both flow systems. There must also be similarity between the surface-boundary conditions and the approach flow wind field. Surface-boundary condition similarity requires equivalence of the following features:

a. Surface-roughness distributions,
b. Topographic relief, and
c. Surface-temperature distribution.

If all the foregoing requirements are met simultaneously, all atmospheric scales of motion ranging from micro- to mesoscale could be simulated within the same flow field. However, all of the requirements cannot be satisfied simultaneously by existing laboratory facilities; thus, a partial or approximate simulation must be used. This limitation requires that atmospheric simulation for plume dispersion must be designed to simulate most accurately those scales of motion which are of greatest significance for the transport and dispersion of plumes.

A.1.2 Partial Simulation of the Atmospheric Boundary Layer

For many fluid modeling situations several of the aforementioned parameters are unnecessarily restrictive and may be relaxed without causing a significant loss in similarity between model and field fluid flow. The Rossby number magnitude controls the extent to which the mean wind direction changes with height. The effect of Coriolis-force-driven lateral wind shear on wind flow is only significant when heights are of the same order of magnitude as the boundary layer height. The Eckert number (in air $Ec = 0.4\ Ma^2\ (T_r/\Delta T_r)$, where Ma is the Mach number) is the ratio of energy dissipation to the convection of thermal energy. Both in the atmosphere and the laboratory flow, the wind velocities and temperature differences are such that the Eckert number is very small; hence, it is neglected. Prandtl number equality guarantees equivalent rates of momentum and heat transport. Since air is the working fluid in both the atmosphere and the laboratory, Prandtl number equality is always maintained.

The approach flow Richardson number (Ri) and Reynolds number (Re) determine the kinematic and dynamic structure of turbulent flow within a boundary layer. This influence is apparent in the variations that occur in the spectral distribution of turbulent kinetic energies with changing Ri and changing Re.

The Reynolds Number

Re equality implies $U_m = (L_p/L_m)U_p$. Re equality at a significantly reduced length scale would cause the model's flow velocity to be above sonic; hence, its equality must be distorted. A reduced Re changes only the higher frequency portion of an Eulerian-type description of the spectral energy distribution. Unfortunately, there is no precise definition as to which portion of an Eulerian Spectrum is dominant in dispersing ground-level or elevated plumes over moderate travel distances.

Most investigators use a minimum Reynolds number requirement based on rough-walled pipe measurements; i.e., $Re = u_* z_o/\nu > 2.5$, where u_*, the friction velocity, and z_o, the roughness length, are derived from a log-linear fit to a measured mean velocity profile. The value 2.5 is an empirically determined constant. At Re below 2.5, it is observed that the mean velocity profiles in turbulent pipe flow lose similarity in shape and deviate from the universal curve of a rough wall turbulent boundary layer. For Re above 2.5, it is observed that the surface drag coefficient (and thus the normalized mean velocity profile) is invariant with respect to increasing Re. For Re between 0.11 and 2.5, the velocity profiles are characteristic of smooth wall turbulent boundary layers. For values below 0.11, the growth of a laminar sublayer on the wall is observed to increase with decreasing Re.

Extrapolation of results from pipe flow measurement to flat plate boundary layers may cause a shift in the magnitude of the minimum Re requirement, but it is generally felt that this shift is small. Precise similarity in the universal form of mean wind shear may be necessary for invariance with respect to the surface drag coefficient, but this does not necessitate that precise similarity must exist for the invariance of the wind field and dispersion. It is the distribution of turbulent velocities which has the greatest effect on the wind field and dispersion. It is the mean wind shear, however, which generates the turbulent velocities. It is possible that the specification of a minimum Re of 2.5 is overly conservative. The criteria, Re > 2.5, for example, is not applicable for flow over complex terrain or building clusters.

The Richardson Number

Although most wind-tunnel investigations are conducted with neutrally stratified boundary layers, there are circumstances when the stratification of the atmosphere must be considered. In particular, air pollution and dispersion problems are often critical during stratified conditions. Unstable stratification may be expected to mitigate hazards by accelerating plume dilution, whereas stable stratification may permit high concentrations to persist. The stability state of the atmosphere is typically characterized by the Richardson number.

The atmospheric gradient Richardson number can be computed from averaged quantities through the equation

$$Ri = g/T\ (\Gamma_d - \Gamma)\ [1 + 0.07/B]\ [(\partial u/\partial z)^2 + (\partial v/\partial z)^2]$$

where Γ and Γ_d are the actual and dry adiabatic potential temperature lapse rates, and $B = [C_p(T_2-T_1)]/[(Z_2-Z_1)(Q_2-Q_1)]$ is the Bowen ratio of sensible to latent heat flux at the surface. The Ri number can be taken to represent the ratio of the relative importance of convective and mechanical turbulence. Negative Ri numbers of large value indicate strong convection and weak mechanical turbulence; zero Ri numbers imply purely mechanical turbulence. Positive Ri numbers less than some critical value, $Ri_{critical}$, suggest the presence of mechanical turbulence damped by the density-induced buoyancy forces; for larger positive Ri numbers, turbulence essentially disappears, since the stratification overpowers production by wind shear. The critical Richardson number has a value near 0.25.

A.1.3 Performance of Prior Fluid Modeling Experiments

Meroney et al. (1978) summarized experimental data available from field and laboratory studies for neutral airflow over hills, ridges, and escarpments. Wind-tunnel model measurements were performed to study the influence of topography profile, surface roughness and stratification on the suitability of various combinations of these variables. Detailed tables of velocity, turbulence intensity, pressure, spectra, etc., were prepared to guide numerical model design and experimental rule of thumb restrictions. Cases included hill slopes from 1:2 to 1:20, neutral and stratified flows, two- and three-dimensional symmetric ridges, six alternate hill and escarpment shapes, and a variety of windward versus leeward slope combinations to evaluate ridge separation characteristics. The laboratory data were validated by comparison with field measurements for flow in the Rakaia Gorge, New Zealand, and over Kahuku Point, Oahu, Hawaii, (Meroney et al., 1978; Chien, Meroney and Sandborn, 1979).

Local heating and cooling of coastline or hill surfaces are the driving mechanisms for sea-land breezes, and anabatic and katabatic winds which may inhibit or enhance airflow over the land surface. Early laboratory work includes simulations of urban heat islands by Yamada and Meroney (1971) and Sethuraman and Cermak (1973), simulation of flow and dispersion at shoreline sites by Meroney et al. (1975a), and simulation of dispersion effects of heat rejected from large industrial complexes by Meroney et al. (1975b).

Meroney (1980) compared three model/field investigations of flow over complex terrain, suggested performance envelopes for realizable modeling in complex terrain, and discussed recent laboratory studies which provide data for valley drainage flow situations. Not all of the model/field comparison experiments performed in the past were successful. Many early studies had model approach flow velocity exponents near zero, were modeled as neutral flows when the field observed strong stratification effects, or simulated unrealistic boundary layer depths, integral scales, or turbulence intensities which did not match their atmospheric counterpart. But few studies claimed unreasonable correlation, and some were strongly self-critical. Nonetheless, most studies accomplished their prestated limited objectives. It would appear that the simulation hypothesis developed in the last few years is appropriate for physical modeling of flow over complex terrain when appropriate care is taken to simulate the approach flow conditions and to maintain simulation parameters equal between model and prototype.

Arya and Plate (1969), Arya (1975) performed velocity, temperature, and turbulence measurements in the lowest 15 percent of a 70 cm deep boundary layer over a smooth surface, where conditions ranged from unstable to moderately stable ($- 0.3 < z/L_{mo} < 0.3$). Free stream flow speeds varied from 3 to 9 m/s, and temperature differences were about 40°C across the boundary layer. Cermak, Shrivastava and Poreh (1983) reported mean velocity and turbulence measurements made for a variety of simulated atmospheric boundary layers over different surface roughness. Free stream flow speeds varied from 2.4 to 3.0 m/s and temperature differences were from 150°C to -80°C across the boundary layer. Poreh and Cermak (1984) reproduced unstable lapse conditions including mixed layers and elevated inversions. They reproduced the characteristics of convective boundary layer turbulence measured in the atmosphere.

Diffusion studies made by Chaudhry and Meroney (1973) in stable boundary layers investigated previously by Arya (1969) have shown agreement of experimental results with Lagrangian similarity theory. Horst (1979) tested Lagrangian similarity predictions of crosswind-integrated ground concentration against the Prairie Grass diffusion experiment (Barad, 1958) and an experiment at Idaho Falls (Islitzer and Dumbauld, 1963). He reported good agreement for all stabilities at distances x/z_o out to $2*10^5$. Poreh and Cermak (1984, 1985) released plumes in their modeled mixing layer. Their plumes exhibited the plume lofting typical of ground sources and the descent typical of elevated sources, predicted from water tank experiments by Willis and Deardorff (1974, 1976, 1978) and numerically by Lamb (1982).

Staff at the Fluid Mechanics Laboratory at the Ecole Centrale de Lyon have studied unstable wind-tunnel boundary layers and compared them with the atmospheric boundary layer (Schon and Mery, 1971). Flow speeds were typically 2 to 4 m/s and the floor temperature was maintained 50°C above ambient. Comparisons with the Kansas data (Haugen et al., 1971) were quite satisfactory, but longitudinal turbulence intensities exhibited a slight Reynolds number dependence, and spectral energy was too low in the high frequency portions of the spectra. The most unstable flow they studied had a Monin-Obukhov scale length of about -1 m at model scales, or -500 to -1000 when scaled to the atmosphere.

A.2 PHYSICAL MODELING OF BLUFF BODY AERODYNAMICS

The interaction of an approach wind field with bluff bodies or structures constructed on the earth's surface is broadly termed "Building Aerodynamics." In a review article on this subject, Meroney (1982) discusses the character of bluff body flow about rectangular buildings and cylindrical cooling towers. Defects in velocity profiles can easily persist from 10 to 15 building heights downwind. Field and laboratory measurements of plume dispersion about the Rancho Seco Nuclear Power

Station in Sacramento, California, confirm that cooling tower wake effects persist for significant downwind distances under a variety of stratification conditions (Allwine, Meroney and Peterka, 1978; Kothari, Meroney and Bouwmeester, 1981).

A.2.1 Simulation Criteria

Often atmospheric turbulence may cause only weak effects compared to the turbulence generated by buildings, obstacles, and terrain. Yet the magnitude of the perturbations depends upon the incident flow turbulence scale and intensity, details of the obstacle shape and surface roughness, and size of the obstacle compared to the boundary layer depth. Geometrical scaling implies that the ratio of the building height to length scale must be matched and, of course, that all other building length scales be reduced to this same ratio.

Several questions should be considered when modeling flows which include surface obstacles:

a. What size obstacles should be disregarded?
b. What detail or roughness on an obstacle need be included?
c. To what upwind distance should all obstacles be included?
d. At what point does the size of a modeled obstacle become too big for the wind tunnel (i.e., blockage effects)?
e. What is the effect on the flow field of mismatching obstacle and approach flow length scales?
f. What is the minimum allowable model obstruction Reynolds number?

Obstacle sizes to be disregarded:

Boundary layer studies of rough surfaces reveal that if protuberances are of a size k, such that $u_*k/\nu < 5$, they will have little effect on the flow in a turbulent boundary layer. Thus, assuming a laboratory wind speed of 1 m/s and a typical friction coefficient $C_f/2 = (u_*/u)^2 = 0.0025$, obstacles of size less than 2 mm would go unnoticed.

Required obstacle surface detail or roughness:

Another question that always arises is "How much detail is required for the building or obstacle model? The answer is, of course, dependent upon the size of the protuberance compared to the plume and the dominant eddies of mixing. If the obstruction is large enough to modify the separated wake over the main obstacle, then it must be included. Often an equivalent obstacle surface roughness suffices. Snyder (1981) concludes a generic surface roughness criterion might be $u_*k/\nu > 20$. For a 1 m/s laboratory flow this results in model roughness elements equal to about 6 mm. But since the exterior flow is usually highly turbulent, the body typically includes a highly unsteady wake, and the u_* value to be used should be that acting on the building surface, rather than that of the approach flow. Hence, even this roughness may be unnecessarily large.

Upstream fetch to be modeled:

Suppose there is another building, tree line, fence, cooling tower, or obstacle some distance, s, upstream of a meteorological measurement location; is it necessary to include this obstacle in the wind-tunnel model? Hunt (1974) showed that the velocity deficit in the wakes of cubes and cylinders is given approximately by:

$$DU_{mx}/U(h) = A\ (s/h)-3/2$$

downwind of the separation bubble, where DU_{mx} is the maximum mean velocity deficit created by the obstacle, h is the height of the obstacle, S is the distance downstream of the obstacle, and A is a constant dependent upon the obstacle shape, orientation, boundary layer thickness, etc. Typically, A = 2.5, but it may range from 1.5 to 5.0. If we desire that the velocity at the spill site be within 3 percent of its undisturbed value, Snyder (1981) recommends that any upstream obstacle as high as s/20 be included upstream in the model of the spill site. If the obstacle's width is much greater than its height (for example, a fence or ridge), one should include it in the physical model if its height is greater than s/100.

Blockage effects:

Because of the influence of wind-tunnel walls on the behavior of the flow past models, it is desirable to use small models or big tunnels, or both. On the other hand, larger models are not only easier to work with, but they may be needed for similarity reasons to achieve large enough Reynolds numbers. It is possible to identify three different types of effects of wind-tunnel constraints. The first is the simple "solid blockage" effect which arises because the fluid stream is unable to expand laterally as it normally would in unconfined flow. The second effect, called "wake blockage", results because the accelerated flow between an obstacle and the tunnel walls continues to "pinch" the wake flow region and reduce its normal lateral rate of growth. The third effect is produced by the growth of boundary layers on the tunnel walls which produce "wall boundary interference." Tunnel blockage can cause separation and reattachment locations to vary, produce higher velocities, larger wake turbulence, and modify the dispersion patterns in the vicinity of obstructions.

The ratio of the cross-sectional area of a model obstacle to that of the tunnel is called the "blockage ratio", BR. Mass continuity produces an average velocity speed-up of S = BR/(1-BR). Although wind tunnels with adjustable ceilings can compensate to some extent by raising the roof locally; this is not a perfect solution to the problem. Measurements on building and cooling tower models placed in different size wind-tunnel test sections reveal major changes in the character of pressure distributions, separation, and wake growth in the presence of flow restricted by wind-tunnel side walls (Farell et al., 1977).

Blockage corrections, which are conventionally applied in aeronautical tunnels, cannot usually be applied to the typical asymmetric model configuration placed against the wall of a meteorological wind tunnel (Ranga Raju and Singh, 1976). Conventional wisdom now suggests the "rule of thumb" that blockage ratios greater than five percent should be avoided.

Simulation of the flow over sharp-edged obstacles:

A number of authors have discussed flow studies about simple cubical or rectangular sharp-edged obstacles. An extensive review about such flow fields and the subsequent character of diffusion near obstacles has been provided by Hosker (1984). Peterka, Meroney and Kothari (1985) describe typical flow deviations which result from the presence of a sharp-edged building.

Consider the main features of the flow around a sharp-edged building. Typically, when the approach flow is normal to the building face, the flow separates from the ground upwind of the building and produces a "horseshoe"-shaped vortex which wraps around the base of the building. The surface streamline reattaches on the front of the building, and fluid parcels move up and down the building's forward face. An elevated streamline flows over the obstacle, dips down behind, and stagnates on the surface at the end of the recirculating cavity immediately downwind of the building. Sometimes separation streamlines from the forward building edges reattach to the same face, yet in other cases the streamlines enter the downwind cavity and mingle with the other recirculating fluid. Air which enters the cavity departs through turbulent mixing across the dividing streamlines, mingles with downwind-pointing vortices and is ejected laterally out of the cavity, or leaves suddenly during an exhalation when the entire cavity appears to collapse and then reform.

When a building is oriented obliquely to the wind, flow over the front side walls does not separate, but strong recirculation occurs on the downwind faces. Flow over the roof often produces counter-rotating "delta-wing" vortices which increase mixing over the top and in the wake of the building. These vortices can cause reattachment of the flow in the middle of the roof and serious plume downwash in the near wake. Other features of the flow near the building include vertical vortices produced by the vertical corners of the building.

Golden (1961) measured the concentration patterns above the roof of model cubes in a wind tunnel. Two sizes of cubes were used to vary the Reynolds number from 1000 to 94,000. The concentration isopleths in the fluid above the cube roof showed only slight variations over the entire range of Reynolds numbers studied. The maximum concentration on the roof itself was found to vary strongly with Reynolds numbers less than 11,000, but to be invariant with Reynolds numbers between 11,000 and 94,000. Frequently, modelers quote Golden's experiments as justification for presuming dispersion invariance when obstacle Reynolds numbers exceed 11,000. However, Golden's "11,000 rule" is limited to the measurement of concentrations at only one point on the roof of smooth-walled cubes placed in a uniform approach flow of very low turbulent intensity. It is probably quite conservative because the shear and high turbulence in a simulated atmospheric boundary layer are likely to further reduce the critical Reynolds number. Indeed, Halitsky (1968) observed that for dispersion in the wake region, no change in isoconcentration isopleths from passive gas releases was found to occur for values of Reynolds number as low as 3300.

Flow around sharp-edged obstacles will remain kinematically similar at very low Reynolds numbers. Wake width variation will be minimal, and obstacle generated turbulence scales and intensity will only vary slowly as Reynolds number decreases. Gas clouds dispersing in this environment will remain similar at very low model speeds.

Simulation of flow over rounded obstacles:

Flow around a smooth cylinder is Reynolds number dependent. This dependence reflects changes in the nature of the boundary layer that forms over the cylinder and its behavior in the vicinity of the flow separation. At low Reynolds numbers, the boundary layer is laminar, and separation occurs easily under the influence of even modest positive pressure gradients. At higher Reynolds numbers, the boundary layer becomes turbulent and flow separation is delayed; i.e., the flow can move farther along a curved surface without separation. At prototype scales, obstacles are large enough that only turbulent separation occurs. However, model flows are usually at such low Reynolds numbers that the local boundary layer growing over a curved surface would be laminar. Most modelers attempt the reproduction of full- scale similarity around curved surfaces by artificially roughening the model surface to force transition to turbulence in these laminar boundary layers. This can be done by providing the surface with special (or artificial) roughness elements, for example, sandpaper, thin wires, or grooves. The height of the roughness, k, should be such that $Uk/\nu > 400$ and $k/R < 0.01$, where U is the mean wind speed at obstacle height, and R is the characteristic obstacle radius of curvature. Szechenyi (1975) studied flows about rough circular cylinders and determined that as Reynolds number decreases, roughening the surface becomes less effective. Fage and Warsap (1929) considered the effect of increasing the surface roughness of cylinders on their drag coefficient. Eventually, even ridiculously large roughness is ineffective.

Niemann and Ruhwedel (1980) compared pressures and forces about a 1:333 scale model to a full-scale hyperbolic cooling tower shell. They roughened their model with vertical ribs of height 0.09 mm and width 0.77 mm, producing a roughness coefficient of $k/2R = 0.0006$ and roughness Reynolds number, $Re_k > 270$. They found meridional forces on the cooling tower model and prototype were similar. Model Reynolds numbers were between $4.5*10^5$ and $6.0*10^5$, and this corresponding to $U_m > 45$ m/s. But again these speeds are much higher than is appropriate for current measurements.

Halitsky et al. (1963) examined dispersion about a smooth-model nuclear reactor containment building (a hemisphere fitted on a vertical cylinder) and found a critical Reynolds number greater than 79,000. (Yet this critical Reynolds number was for flow very close to the vessel wall. The behavior of concentration isopleths further downwind is likely to be less Reynolds number dependent.)

Although the details of fluid motions around rounded obstacles vary significantly with Reynolds number, the gross features of the flow do not change. Even small models at low wind speeds will produce horseshoe-shaped ground vortices, elevated pairs, and regular vortex shedding. If the internal boundary layer over the obstacle is laminar, then the wake region will be broader and less intense.

A.2.2 Performance of Prior Fluid Modeling Experiments

A number of studies have been performed in the Colorado State University Fluid Dynamics and Diffusion Laboratory to establish the effect of buildings and meteorological masts on flow fields. Hatcher et al. (1977) examined flow and dispersion in stratified flow downwind of the Experimental Organic Cooled Reactor, Idaho Falls; Allwine et al. (1978) studied the Rancho Seco Reactor, Sacramento; Kothari et al. (1981) studied the Duane Arnold Energy Center, Iowa. In each case field measurements were compared to laboratory measurements with good agreement. Specific effects of the structure of a meteorological mast on instrumentation response were reported by Hsi and Cermak (1965).

A.3 PHYSICAL MODEL OF PLUME MOTION

In addition to modeling the turbulent structure of the atmosphere in the vicinity of a test site it is necessary to properly scale the plume source conditions. One approach would be to follow the methodology used in Section 2.1; i.e., writing the conservation statements for the combined flow system followed by fractional analysis to find the governing parameters. An alternative approach, the one which will be used here, is that of similitude (Kline, 1965). The method of similitude obtains scaling parameters by reasoning that the mass ratios, force ratios, energy ratios, and property ratios should be equal for both model and prototype. When one considers the dynamics of gaseous plume behavior the following nondimensional parameters of importance are identified.[1]

$$\text{Mass Flux Ratio} = \frac{\text{mass flow of plume}}{\text{effective mass flow of air}}$$

---

[1] The scaling of plume Reynolds number is also a significant parameter. Its effects are invariant over a large range. This makes it possible to accurately model its influence by maintaining model tests above a minimum plume Reynolds number requirement.

Momentum Flux Ratio = $\frac{\text{inertia of plume}}{\text{effective inertia of air}}$

Densimetric Froude No. (relative to the inertia of the air) = $\frac{\text{effective inertia of air}}{\text{buoyancy of plume}}$

Densimetric Froude No. (relative to the inertia of the plume) = $\frac{\text{inertia of plume}}{\text{buoyancy of plume}}$

Flux Froude No. = $\frac{\text{momentum flux of air}}{\text{buoyancy momentum flux of plume}}$

Volume Flux Ratio = $\frac{\text{volume flow of plume}}{\text{effective volume flow of air}}$

It is necessary to maintain equality of the plume's specific gravity, ρ_g/ρ_a, over the plume's entire lifetime to obtain simultaneous simulation of all of these parameters. Unfortunately a requirement for equality of the plume gas specific gravity for plume with significant buoyancy differences (i.e. ρ_g not equal ρ_a) leads to several complications in practice. These are:

1) Equality of the source gas specific gravity between a model and its atmospheric equivalent leads to a wind speed scaling from $(U_m/U_p)^2 = L_m/L_p$. For a significant range of atmospheric wind speeds this relationship leads to wind- tunnel speeds at which there is a possible loss of the Reynolds number invariance in the approach flow.

2) A thermal plume in the atmosphere is frequently simulated in the laboratory by an isothermal plume formed from a gas of appropriate molecular weight. Under certain situations of specific heat capacity mismatch, this practice will lead to a variation of the equality of plume density as the plume mixes with air.

It is important to examine each modeling situation and decide if an approximation to complete plume behavior may be employed without a significant loss in the similarity of the modeled plume structure.

REFERENCES

Allwine, K. J., Meroney, R. N., and Peterka, J. A. (1978), "Rancho Seco Building Wake Effects on Atmospheric Diffusion: Simulation in a Meteorological Wind Tunnel," FDDL Report No. CER77-78KJA-RNM-JAP25, Colorado State University, Fort Collins, Colorado.

Arya, S. P. S., and Plate, E. J. (1969), "Modeling of the Stably Stratified Atmospheric Boundary Layer," J. Atmos. Sci., Vol. 26, No. 4, pp. 656-665.

Ayra, S. P. S. (1975), "Buoyancy Effects in a Horizontal Flat-Plate Boundary Layer," J. Fluid Mech., Vol. 68, Pt. 2, pp. 321-343.

Barad, M. L., Ed. (1958), Project Prairie Grass: A Field Program in Diffusion, Geophysical Research Papers, No. 59, Vols. I and II, Report AFCRC-TR-58-235, Air Force Cambridge Research Center.

Brunn, (1978), "Multi-Probes and Higher Moments," Proceedings of the Dynamic Flow Conference 1978, pp. 943-961.

Cermak, J. E. (1975), "Applications of Fluid Mechanics to Wind Engineering--A Freeman Scholar Lecture," J. of Fluids Engineering, Vol. 97, pp. 9-38.

Cermak, J. E., Shrivastava, P. K., and Poreh, M. (1983), "wind-tunnel Research on the Mechanics of Plumes in the Atmospheric Surface Layer," Civil Engineering Department Report CER83-84JEC-PKS-MP12, Colorado State University, Fort Collins, CO, Annual Progress Report to U.S. Dept. of Army Contract DAAK11-82-K-0004, 140 pp.

Chaudhry, F. H. and Meroney, R. N. (1973), "A Laboratory Study of Diffusion in Stably Stratified Flow," Atmos. Envir., Vol. 7, pp. 443-454. Chien, H. C., Meroney, R. N., and Sandborn, V. A. (1979), "Sites for Wind-Power Installations: Physical Modeling of the Wind Field Over Kahuku Point, Hawaii," FDDL Report No. CER79-80HCC-RNM-VAS25, Colorado State University, Fort Collins, Colorado.

Counihan, J. (1975), "Adiabatic Atmospheric Boundary Layers: A Review and Analysis of Data from the Period 1880-1972," Atmos. Envir., Vol. 9, pp. 871-905.

Fage, A. and Warsap, J. H. (1929), "Effects of Turbulence and Surface Roughness on Drag of Circular Cylinders," U.K., ARC R&M 1283.

Farell, C., Carrasquel, S., Guven, O., and Patel, V. C. (1977), "Effect of Wind-Tunnel Walls on the Flow Past Circular Cylinders and Cooling Tower Models," J. of Fluids Engineering, Vol. 99, pp. 470-479.

Gifford, F. A. (1976), Turbulent Diffusion-Typing Schemes: A Review, Nucl. Saf., Vol. 17, No. 1, pp. 72 ff.

Golden, J. (1961), "Scale Model Techniques," M.S. Thesis, Dept. of Met. and Ocean., New York University, 42 pp.

Golder, D. G. (1972), "Relations Among Stability Parameters in the Surface Layer," Boundary-Layer Meteorol., Vol. 3, No. 1, pp. 47-58.

Halitsky, J., Colden, J., Halpern, P., and Wu, P. (1963), "Wind Tunnel Tests of Gas Diffusion from a Leak in the Shell of a Nuclear Power Reactor and from a Nearby Stack," N.Y.U. Meteorol. and Oceanog. Geophys. Sciences Lab. Report 63-2 (New York Univ., College of Engineering, New York.)

Halitsky, J. (1968), "Gas Diffusion Near Buildings," Meteorology and Atomic Energy, 1968, editor D. H. Slade, Atomic Energy Commission, Ch. 5-5, pp. 221-256.

Hatcher, R. V. and Meroney, R. N. (1977), "Dispersion in the Wake of a Model Industrial Complex," Joint Conf. on Applications of Air Pollution Meteorology, Proceedings, Am. Meteorol. Sco., Salt Lake City, Utah, 29 November - 2 December, 1977, pp. 343-346.

Haugen, D. A., Kaimal, J. C., and Bradley, E. F. (1971), "an Experimental Study of Reynolds Stress and Heat Flux in the Atmospheric Surface Layer," Quart. J. Roy. Meteorol. Soc., Vol. 97, pp. 168-180.

Hinze, J. O. (1975), Turbulence, McGraw-Hill, New York, 2nd. edition, 790 pp.

Horst, T. W. (1979), "Lagrangian Similarity Modeling of Vertical Diffusion from a Ground Level Source," J. Appl. Meteorol., Vol. 18, pp. 733-740.

Hosker, R. P., Jr. (1984), "Flow and Diffusion Near Obstacles," Atmospheric Science and Power Production, DOE/TIC-27601, pp. 241-326.

Hsi, G., and Cermak, J. E. (1965), "Meteorological-Tower Induced Wind Field Perturbations," Prepared under U.S. Army Research Grant DA-AMC-28-043-64-G-9, Fluid Mechanics Program Report No. CER65GH-JEC49, Colorado State University, Fort Collins, Colorado.

Hunt, J. C. R. (1974), "Wakes Behind Buildings," presented at the Aeronautical Research Council's Atmospheric Environment Committee Meeting, Oct. 23, ARC Report 35601, Atmos. 229, Aeronautical Research Council of Great Britain, Her Majesty's Stationery Office, London.

Hunt, J. C. R., Snyder, W. H., and Lawson, F. E., Jr. (1978), "Flow Structure and Turbulent Diffusion around a Three-Dimensional Hill: Fluid Modeling Study on Effects of Statification: Part I: Flow Structure," Envir. Prot. Agcy. Report No. EPA 600/4-78-041, Fesearch Triangle Park, NC, 84 pp.

Islitzer, N. F. and Dumbauld, R. K. (1963), "Atmospheric Diffusion Deposition Studies over Flat Terrain," INt. J. Air Water Pollut., Vol. 7 (11-12), pp. 999-1022.

Kline, S. J. (1965), Similitude and Approximation Theory, McGraw-Hill Book Company, New York, 229 pp.

Kothari, K. M., Meroney, R. N., Bouwmeester, (1981), "An Algorithm to Estimate Field Concentrations Under Nonsteady Meteorological Conditions from Wind Tunnel Experiments," Jornal of Applied Meteorology, Vol. 30, pp. 92-101.

Kothari, K. M., Meroney, R. N. and Peterka, J. A. (1979), "Nuclear Power Plant Building Works Effects on Atmosphere Diffusion," EPRI Report No. 1891, CER79-80KMK-RNM-JAP28, 109 pp.

Lamb, R. G. (1982), "Diffusion in the Convective Boundary Layer," Chapter 5, Atmospheric Turbulence and Air Pollution Modeling, Nieuwstadt and van Dop, editors, D. Reidel Publishing Company, Dordrecht, Holland, pp. 159-230.

Meroney, R. N. (1980), "Wind-Tunnel Simulations of the Flow Over Hills and Complex Terrain," J. of Industrial Aerodynamics, Vol. 5, pp. 297-321.

Meroney, R. N. (1982), "Turbulent Diffusion Near Buildings," Engineering Meteorology, Chapter 11, pp. 481-521.

Meroney, R. N., Cermak, J. E., and Garrison, J. A. (1975a), "Wind-Tunnel Study of Stack Gas Dispersal at Lansing Power Station, Units 1, 2, 3, and 4," FDDL Report No. CER74-75RNM-JEC-JAG28, Colorado State University, Fort Collins, Colorado.

Meroney, R. N., Cermak, J. E., and Garrison, J. A. (1975b), "Wind-Tunnel Study of Stack Gas Dispersal at Lansing Power Station, Units 1, 2, 3, and 4," FDDL Report No. CER74-75RNM-JEC-JAG29, Colorado State University, Fort Collins, Colorado.

Meroney, R. N., Sandborn, V. A., Bouwmeester, R. J. B., Chien, H. C., and Rider, M. (1978), "Sites for Wind-Power Installations: Physical Modeling of the Influence of Hills, Ridges and Complex Terrain - Part II: Executive Summary," Dept. of Energy Report RLO/2438-77/3, 90 pp.

Neff, D. E., Tan T. Z., and Meroney, R. N. (1988), "Fluid Modeling of Exhaust Gas Dispersion from the Parcel 7 Ventilation Site, Central Artery/Third Harbor Tunnel Project," FDDL Report No. CER88-DEN-RNM-6, Colorado State University, Fort Collins, Colorado.

Niemann, H. J. and Ruhwedel, J. (1980), "Full-scale and Model Tests on Wind-induced, Static and Dynamic Stresses in Cooling Tower Shells," Eng. Struct., Vol. 2, pp. 81-89.

Ogawa, Y., Diosey, P. G., Uehara, K., and Ueda, H. (1985), "Wind Tunnel Observation of Flow and Diffusion Under Stable Stratification," Atmos. Envir., Vol. 19, pp. 65-74.

Peterka, J. A., Meroney, R. N. and Kothari, K. (1985), "Wind Flow Patterns About Buildings," J. of Wind Engineering and Industrial Aerodynamics, Vol. 21, pp. 21-38.

Plate, E. J. and Cermak, J. E. (1963), "Micro-meteorological Wind-Tunnel Facility," Fluid Dynamics and Diffusion Laboratory Report CER63EJP-JEC9, Colorado State University, Fort Collins, Colorado, 65 pp.

Poreh, M. and Cermak, J. E. (1984), "Wind Tunnel Research on the Mechanics of Plumes in the Atmospheric Surface Layer, Part II," Annual Report to U.S. Dept. of Army, Chemical Systems Laboratory, Aberdeen Proving Ground, Maryland, Colorado State University Civil Engineering Department Report CER84-85MP-JEC47, 45 pp.

Fanga Raju, K. G. and Singh, V. (1976), "Blockage Effects on Drag of Sharp Edged Bodies," J. of Industrial Aerodynamics, Vol. 1, pp. 301-309.

Schlichting, H. (1968), Boundary Layer Theory, McGraw-Hill Book Company, New York, 774 pp.

Schon, J. P. and Mery, P. (1971), "A Preliminary Study of the Simulation of Neutral Atmospheric Boundary Layer Using Air Injection in a Wind Tunnel," Atmos. Enviro., Vol. 5, No. 5, pp. 299-312.

Sethurama, S., and Cermak, J. E. (1973), "Stratified Shear Flows Over a Simulated Three-Dimensional Urban Heat Island," Project Themis Technical Report No. 23, CER73-74SS-JEC4, Colorado State University, Fort Collins, Colorado.

Snyder, W. H., Britter, R. E., and Hunt, J. C. R. (1979), "A Fluid Modeling Study of the Flow Structure and Plume Impingement on a Three-Dimensional Hil in Stably Stratified Flow," Proc. Fifth Int. Conf. on Wind Engr., Pergamon Press, NY, Vol. 1, pp. 319-329

Snyder, W. H. (1981), "Guidelines for Fluid Modeling of Atmospheric Diffusion," EPA Report EPA-600/8-81-009, 185 pp.

Szechenyi, E. (1975), "Supercritical Reynolds Number Simulation for Two dimensional Flow over Circular Cylinders," J. Fluid Mech., Vol. 70, pp. 529-542.

Teunissen, H. W. (1975), "Simulation of the Planetary Boundary Layer in a Multiple Jet Wind Tunnel," Atmos. Envir., Vol. 9, pp. 145-174.

Willis, G. E. and Deardorff, J. W. (1974), "A Laboratory Model of the Unstable Planetary Boundary Layer," J. Atmos. Sci., Vol. 31, pp. 1297-1307.

Willis, G. E. and Deardorff, J. W. (1976), "A Laboratory Model of Diffusion into the Convective Planetary Boundary Layer," Quart. J. Roy. Meteorol. Soc., Vol. 102, pp. 427-445.

Willis, G. E. and Deardorff, J. W. (1978), "A Laboratory Study of Dispersion from an Elevated Source Within a Modeled Convective Planetary Boundary Layer," Atmos. Envir., Vol. 12, pp. 1305-1311.

Yamada, T. and Meroney, R. N. (1971). "Numerical and Wind-Tunnel Simulation of Response of Stratified Shear Layers to Nonhomogeneous Surface Features," CER7071TY-RNM62, Colorado State University, also (AD-730-953).

Table 1 Velocity Profile Conditions

Profile #	X Position	Y Position	Model Wind Direction (from N)	Reference Velocity mps @ 1m
1	Upwind (Land)	Tunnel Center	180	0.9
2	Upwind (Land)	Tunnel Center	180	1.6
3	Upwind (Sea)	Tunnel Center	45	1.2
4	Upwind (Sea)	Tunnel Center	45	0.8
5	Model Center	Model Center	0	1.6
6	Model Center	Model Center	45	1.3
7	Model Center	Model Center	90	1.2
8	Model Center	Model Center	135	1.6
9	Model Center	Model Center	180	1.6
10	Model Center	Model Center	225	1.7
11	Model Center	Model Center	270	1.7
12	Model Center	Model Center	315	1.7

note: Model values for distance and velocity are used here.

Table 2 Velocity Profile Data for Profiles 1, 2, 3 and 4

	--- Profile: No.1 ---		--- Profile: No.2 ---		--- Profile: No.3 ---		--- Profile: No.4 ---	
Normalized Height	Normalized Velocity	Turbulent Intensity (%)	Normalized Velocity	Turbulent Intensity (%)	Normalized Velocity	Turbulent Intensity (%)	Normalized Velocity	Turbulent Intensity (%)
0.025	0.310	32.6	0.285	34.7	0.544	17.2	0.529	17.4
0.032	0.356	33.7	0.319	33.5	0.527	20.5	0.588	15.6
0.040	0.358	29.2	0.365	32.4	0.546	17.3	0.611	16.8
0.050	0.413	28.0	0.393	32.8	0.591	17.7	0.658	14.3
0.060	0.475	29.6	0.395	31.2	0.609	17.0	0.643	14.6
0.080	0.491	26.9	0.481	22.8	0.635	16.2	0.689	13.9
0.097	0.568	24.3	0.532	23.5	0.648	16.7	0.686	15.1
0.122	0.601	20.9	0.565	21.9	0.679	13.7	0.682	16.0
0.150	0.680	16.8	0.631	17.3	0.703	12.8	0.754	10.8
0.177	0.709	16.3	0.698	16.1	0.747	13.2	0.751	11.4
0.197	0.768	11.8	0.690	14.3	0.743	13.8	0.781	9.8
0.252	0.806	10.8	0.779	12.2	0.778	14.1	0.766	12.5
0.297	0.846	10.7	0.776	11.4	0.808	12.0	0.841	9.7
0.400	0.892	8.5	0.858	8.6	0.887	9.1	0.860	7.8
0.500	0.921	6.9	0.884	6.9	0.924	7.3	0.926	5.9
0.600	0.934	6.7	0.913	6.1	0.938	6.4	0.932	4.6
0.800	0.993	4.8	0.945	5.7	0.966	5.1	0.943	4.1
1.000	1.000	5.4	0.999	5.4	1.002	4.6	0.999	4.1
1.200	1.024	4.9	1.030	5.4	1.035	5.2	1.036	5.6

Reference Height = 1260 ft.

Table 3 Velocity Profile Data for Profiles 5, 6, 7 and 8

	--- Profile: No.5 ---		--- Profile: No.6 ---		--- Profile: No.7 ---		--- Profile: No.8 ---	
Normalized Height	Normalized Velocity	Turbulent Intensity (%)	Normalized Velocity	Turbulent Intensity (%)	Normalized Velocity	Turbulent Intensity (%)	Normalized Velocity	Turbulent Intensity (%)
0.025	0.437	30.4	0.467	25.6	0.608	13.8	0.168	45.8
0.032	0.454	30.1	0.473	27.0	0.624	14.0	0.190	62.6
0.040	0.409	34.8	0.502	23.6	0.620	14.2	0.187	48.1
0.050	0.426	31.4	0.490	22.8	0.646	12.7	0.203	51.7
0.060	0.414	32.0	0.524	20.4	0.672	14.1	0.212	56.0
0.080	0.368	38.3	0.500	20.7	0.693	13.6	0.226	48.7
0.097	0.362	38.3	0.494	19.4	0.729	11.0	0.314	46.7
0.122	0.298	40.3	0.503	22.0	0.759	13.0	0.430	35.7
0.150	0.303	40.4	0.544	23.6	0.748	11.5	0.454	35.8
0.177	0.282	40.9	0.621	24.4	0.763	11.6	0.553	24.7
0.197	0.249	37.7	0.699	22.0	0.767	12.4	0.593	21.3
0.252	0.245	38.8	0.843	12.8	0.815	10.6	0.646	21.8
0.297	0.232	40.1	0.935	8.5	0.831	10.4	0.699	16.1
0.400	0.268	54.0	0.909	8.8	0.886	8.5	0.798	10.6
0.500	0.574	42.2	0.925	7.3	0.913	7.5	0.860	8.3
0.600	0.979	10.0	0.984	4.8	0.950	5.7	0.876	7.7
0.800	1.009	5.4	0.983	4.2	0.990	4.4	0.943	5.5
1.000	0.999	4.2	0.999	4.1	1.002	4.7	1.001	4.6
1.200	1.046	5.2	0.992	4.2	1.053	5.0	1.013	4.9

Reference Height = 1260 ft.

Table 4 Velocity Profile Data for Profiles 9, 10, 11 and 12

	--- Profile: No.9 ---		--- Profile: No.10 --		--- Profile: No.11 --		--- Profile: No.12 ---	
Normalized Height	Normalized Velocity	Turbulent Intensity (%)	Normalized Velocity	Turbulent Intensity (%)	Normalized Velocity	Turbulent Intensity (%)	Normalized Velocity	Turbulent Intensity (%)
0.025	0.286	43.2	0.124	31.4	0.198	43.5	0.121	30.2
0.032	0.323	36.3	0.130	32.4	0.198	47.1	0.125	30.5
0.040	0.353	34.5	0.150	38.9	0.186	46.2	0.135	34.1
0.050	0.357	32.2	0.167	46.4	0.206	44.0	0.148	30.3
0.060	0.383	29.6	0.223	44.5	0.222	39.8	0.164	35.5
0.080	0.460	27.4	0.344	34.7	0.234	35.5	0.185	31.7
0.097	0.481	23.1	0.439	29.4	0.267	31.6	0.205	28.5
0.122	0.538	18.4	0.533	27.0	0.243	36.3	0.218	32.6
0.150	0.537	17.8	0.575	26.6	0.211	39.2	0.254	30.5
0.177	0.566	20.8	0.568	25.8	0.187	42.8	0.290	37.0
0.197	0.625	18.9	0.613	24.7	0.204	42.7	0.324	34.0
0.252	0.719	13.8	0.622	23.5	0.245	48.1	0.459	28.7
0.297	0.749	14.8	0.704	21.4	0.399	42.0	0.522	27.2
0.400	0.822	9.5	0.869	11.7	0.697	26.6	0.721	18.2
0.500	0.879	9.1	0.931	7.2	0.885	13.4	0.878	14.9
0.600	0.917	7.0	0.945	5.7	0.910	8.9	0.999	6.3
0.800	0.961	5.0	0.979	5.0	0.994	4.5	1.004	4.8
1.000	0.998	4.2	0.998	4.4	1.000	4.0	0.997	4.0
1.200	1.050	5.0	1.026	4.1	1.022	4.5	1.043	4.6

Reference Height = 1260 ft.

Table 5 Visualization Test Conditions

Run No.	Vent Site	Building Height $(ft)_p$	Stack Height $(ft)_p$	Exit Velocity $(fpm)_p$	Wind Dir. (from)
1	Bos-Ed (2B)	156	240	800	SSE
2	Bos-Ed (2B)	156	240	800	S
3	Bos-Ed (2B)	156	240	800	SSW
4	Bos-Ed (2B)	156	240	1600	SSW
5	Bos-Ed (2B)	156	240	800	NW
6	Bos-Ed (2B)	156	240	1600	NW
7	Atlantic (3)	156	240	800	SSE
8	Atlantic (3)	156	240	800	SSW
9	J. Hook (4)	156	240	800	SSW
10	J. Hook (4)	156	240	1600	SSW
11	J. Hook (4)	156	240	1600	NW
12	J. Hook (4)	156	240	800	NNW
13	Appraiser(5)	156	240	800	SSW
14	Appraiser(5)	156	240	1600	SSW
15	Bos-Ed (2B)	156	240	800	NNE
16	Bos-Ed (2B)	156	240	800	NE
17	Bos-Ed (2B)	156	240	1600	NE
18	Bos-Ed (2B)	156	240	800	E
19	Bos-Ed (2B)	156	240	800	SE
20	Bos-Ed (2B)	156	240	1600	SE
21	Atlantic (3)	156	240	800	NE
22	Atlantic (3)	156	240	800	E
23	Atlantic (3)	156	240	800	SE
24	J. Hook (4)	156	240	800	NE
25	J. Hook (4)	156	240	1600	NE
26	J. Hook (4)	156	240	800	ENE
27	J. Hook (4)	156	240	800	ESE
28	J. Hook (4)	156	240	800	SE
29	Appraiser(5)	156	240	800	NE
30	Appraiser(5)	156	240	800	E
31	Appraiser(5)	156	240	800	ESE

Table 6 Visual Test Results Summary

Run No.	Vent Site	Bldg Height (ft)	Stack Height (ft)	Exit Velocity (fpm)	Wind Dir (from)	Stack Downwash	Observed Plume Behavior: Building Downwash	Cavity Mixing	Plume Descent	Plume Lofting	Skyscpr Impingt
1	2B	156	240	800	SSE	X	X		X		X
2	2B	156	240	800	S	X	X		X		
3	2B	156	240	800	SSW	X	X		X		
4	2B	156	240	1600	SSW	X					
5	2B	156	240	800	NW	X	X	X	X		
6	2B	156	240	1600	NW	X	X	X			
7	3	156	240	800	SSE	X	X		X		X
8	3	156	240	800	SSW	X	X		X		
9	4	156	240	800	SSW	X	X		X		
10	4	156	240	1600	SSW	X				X	
11	4	156	240	1600	NW	X		X			
12	4	156	240	800	NNW	X	X	X	X		
13	5	156	240	800	SSW	X			X		
14	5	156	240	1600	SSW	X				X	
15	2B	156	240	800	NNE	X	X	X	X		
16	2B	156	240	800	NE	X	X	X	X		
17	2B	156	240	1600	NE	X	X				
18	2B	156	240	800	E	X	X	X	X		X
19	2B	156	240	800	SE	X	X	X			X
20	2B	156	240	1600	SE	X	X			X	X
21	3	156	240	800	NE	X	X		X		
22	3	156	240	800	E	X	X	X	X		X
23	3	156	240	800	SE	X	X	X			X
24	4	156	240	800	NE	X	X		X		
25	4	156	240	1600	NE	X			X		
26	4	156	240	800	ENE	X	X		X		X
27	4	156	240	800	ESE	X	X	X	X		X
28	4	156	240	800	SE	X	X	X	X		X
29	5	156	240	800	NE	X			X		
30	5	156	240	800	E	X	X		X		X
31	5	156	240	800	ESE	X	X	X	X		X

Table 7 Concentration Sampling Locations

Point No.	Code No.	Description of Receptor Site	Field Distance (ft)	Field Direction (Degrees)	Field Height (ft)	Model Distance (in)	Model Height (in)
1	A7	Sheraton Bldg (roof)	0	0	203.0	0.0	6.3
2	A1	Harbor Towers (plume ht.)	1250	12	240.0	39.1	7.5
3	A2	Harbor Towers (pool)	1175	15	0.0	36.7	0.0
4	A3	Boston Harbor Hotel	760	21	167.0	23.8	5.2
5	A4	US Customs Bldg (Street)	390	22	0.0	12.2	0.0
6	A5	Rowe's Wharf	1075	31	89.1	33.6	2.8
7	A6	US Customs Bldg (roof)	450	32	139.6	14.1	4.4
8	B1	Northern Ave. & Sleeper St.	840	96	0.0	26.3	0.0
9	B2	Victoria Station Rest.	760	123	0.0	23.8	0.0
10	B3	Farnsworth Street	1250	135	0.0	39.1	0.0
11	B4	SE	1970	135	0.0	61.6	0.0
12	B5	Children's Museum	920	141	0.0	28.8	0.0
13	B6	Congress Street	1400	152	0.0	43.8	0.0
14	B7	Boston Tea Party Museum	640	172	0.0	20.0	0.0
15	B8	S (Necco St.)	1970	180	0.0	61.6	0.0
16	C1	Congress ST. & Dorchester Ave	710	200	0.0	22.2	0.0
17	C2	Dorchester Ave. & Summer ST.	1025	202	0.0	32.0	0.0
18	C3	Stone & Webster Bldg.	1140	213	226.0	35.6	7.1
19	C5	Fed Reserve intake # 3	920	230	537.5	28.8	16.8
20	C6	Stearns Perry & Smith Co.	440	233	99.7	13.8	3.1
21	C7	South Station	1225	235	93.1	38.3	2.9
22	C8	Fed Reserve Intake # 2	960	236	97.5	30.0	3.0
23	C9	South Station (Street)	1200	240	0.0	37.5	0.0
24	C4	Dewey Square (roof)	1536	247	610.0	48.0	19.1
25	C10	Dewey Square (Street	1250	247	0.0	39.1	0.0
26	C11	Fed Reserve (Street)	630	248	0.0	19.7	0.0
27	C12	Keystone Bldg (Intake)	775	269	191.7	24.2	6.0
28	C13	Keystone Bldg. (Street)	780	269	0.0	24.4	0.0
29	D1	Bldg betw High St. & Matthews	970	275	411.7	30.3	12.9
30	D2	Western Union Bldg	640	277	187.0	20.0	5.8
31	D3	Road House	600	281	40.0	18.8	1.3
32	D4	125 High Street Bldg	630	294	226.0	19.7	7.1
33	D5	New England T & T	1075	297	364.5	33.6	11.4
34	D6	New Fire House	450	307	24.0	14.1	0.8
35	D8	NW (Milk ST.)	1550	308	0.0	48.4	0.0
36	D7	State Street Bank Bldg.	900	315	443.3	28.1	13.9
37	D9	Oliver St. & Franklin St.	1125	320	0.0	35.2	0.0
38	D10	21 Story Tower	650	324	230.0	20.3	7.2
39	D11	Oliver St. & High St.	850	324	0.0	26.6	0.0
40	D12	Shops on Purchase & Olive	450	329	70.7	14.1	2.2
41	D17	Bldg on India & Milk (Roof)	1625	340	164.2	50.8	5.1
42	D13	International Place (Street)	510	348	0.0	15.9	0.0
43	D14	International Place (Intake)	600	350	42.0	18.8	1.3
44	D16	Bldg. on Broad & High (Roof)	975	353	82.2	30.5	2.6
45	D15	N (Atlantic Ave.)	1970	358	0.0	61.6	0.0

Table 8 Concentration Test Conditions

Run No.	Vent Site	FIELD VALUES Stack Height (ft)	Exit Speed (fpm)	Wind Speed mps@30m	Wind Dir. (from)	Approach Roughness	MODEL VALUES Wind Speed cm/s@7.8	Exhaust Flow (ccs)
1	Bos-Ed.	240	400	5.0	NE	Sea	50	196
2	Bos-Ed.	240	1600	5.0	NE	Sea	50	786
3	Bos-Ed.	240	400	5.0	ENE	Sea	50	196
4	Bos-Ed.	240	1600	5.0	ENE	Sea	50	786
5	Bos-Ed.	240	400	5.0	SSW	Land	50	196
6	Bos-Ed.	240	1600	5.0	SSW	Land	50	786
7	Bos-Ed.	300	400	5.0	NE	Sea	50	196
8	Bos-Ed.	300	1600	5.0	NE	Sea	50	786
9	Bos-Ed.	300	400	5.0	ENE	Sea	50	196
10	Bos-Ed.	300	1600	5.0	ENE	Sea	50	786
11	Bos-Ed.	300	400	5.0	SSW	Land	50	196
12	Bos-Ed.	300	1600	5.0	SSW	Land	50	786
13	J. Hook	240	400	5.0	NE	Sea	50	196
14	J. Hook	240	1600	5.0	NE	Sea	50	786
15	J. Hook	240	400	5.0	60	Sea	50	196
16	J. Hook	240	1600	5.0	60	Sea	50	786
17	J. Hook	240	400	5.0	190	Land	50	196
18	J. Hook	240	1600	5.0	190	Land	50	786
19	J. Hook	300	400	5.0	NE	Sea	50	196
20	J. Hook	300	1600	5.0	NE	Sea	50	786
21	J. Hook	300	400	5.0	60	Sea	50	196
22	J. Hook	300	1600	5.0	60	Sea	50	786
23	J. Hook	300	400	5.0	190	Land	50	196
24	J. Hook	300	1600	5.0	190	Land	50	786
25	Bos-Ed.	300	400	5.0	N	Land	50	196
26	Bos-Ed.	300	400	5.0	NNE	Sea	50	196
27	Bos-Ed.	300	400	5.0	NE	Sea	50	196
28	Bos-Ed.	300	400	5.0	ENE	Sea	50	196
29	Bos-Ed.	300	400	5.0	E	Sea	50	196
30	Bos-Ed.	300	400	5.0	ESE	Sea	50	196
31	Bos-Ed.	300	400	5.0	SE	Sea	50	196
32	Bos-Ed.	300	400	5.0	SSE	Land	50	196
33	Bos-Ed.	300	400	5.0	S	Land	50	196
34	Bos-Ed.	300	400	5.0	SSW	Land	50	196
35	Bos-Ed.	300	400	5.0	SW	Land	50	196
36	Bos-Ed.	300	400	5.0	WSW	Land	50	196
37	Bos-Ed.	300	400	5.0	W	Land	50	196
38	Bos-Ed.	300	400	5.0	WNW	Land	50	196
39	Bos-Ed.	300	400	5.0	NW	Land	50	196
40	Bos-Ed.	300	400	5.0	NNW	Land	50	196
41	Bos-Ed.	300	800	5.0	N	Land	50	393
42	Bos-Ed.	300	800	5.0	NNE	Sea	50	393
43	Bos-Ed.	300	800	5.0	NE	Sea	50	393
44	Bos-Ed.	300	800	5.0	ENE	Sea	50	393
45	Bos-Ed.	300	800	5.0	E	Sea	50	393
46	Bos-Ed.	300	800	5.0	ESE	Sea	50	393
47	Bos-Ed.	300	800	5.0	SE	Sea	50	393
48	Bos-Ed.	300	800	5.0	SSE	Land	50	393
49	Bos-Ed.	300	800	5.0	S	Land	50	393
50	Bos-Ed.	300	800	5.0	SSW	Land	50	393
51	Bos-Ed.	300	800	5.0	SW	Land	50	393
52	Bos-Ed.	300	800	5.0	WSW	Land	50	393
53	Bos-Ed.	300	800	5.0	W	Land	50	393
54	Bos-Ed.	300	800	5.0	WNW	Land	50	393
55	Bos-Ed.	300	800	5.0	NW	Land	50	393
56	Bos-Ed.	300	800	5.0	NNW	Land	50	393
57	Bos-Ed.	300	1600	5.0	N	Land	50	786
58	Bos-Ed.	300	1600	5.0	NNE	Sea	50	786
59	Bos-Ed.	300	1600	5.0	NE	Sea	50	786
60	Bos-Ed.	300	1600	5.0	ENE	Sea	50	786
61	Bos-Ed.	300	1600	5.0	E	Sea	50	786
62	Bos-Ed.	300	1600	5.0	ESE	Sea	50	786
63	Bos-Ed.	300	1600	5.0	SE	Sea	50	786
64	Bos-Ed.	300	1600	5.0	SSE	Land	50	786
65	Bos-Ed.	300	1600	5.0	S	Land	50	786
66	Bos-Ed.	300	1600	5.0	SSW	Land	50	786
67	Bos-Ed.	300	1600	5.0	SW	Land	50	786

Table 9 Concentration Test Conditions (continued)

		FIELD VALUES					MODEL VALUES	
Run No.	Vent Site	Stack Height (ft)	Exit Speed (fpm)	Wind Speed mps@30m	Wind Dir. (from)	Approach Roughness	Wind Speed cm/s@7.8	Exhaust Flow (ccs)
68	Bos-Ed.	300	1600	5.0	WSW	Land	50	786
69	Bos-Ed.	300	1600	5.0	W	Land	50	786
70	Bos-Ed.	300	1600	5.0	WNW	Land	50	786
71	Bos-Ed.	300	1600	5.0	NW	Land	50	786
72	Bos-Ed.	300	1600	5.0	NNW	Land	50	786
73	Bos-Ed.	300	3200	5.0	NNE	Sea	50	1572
74	Bos-Ed.	300	3200	5.0	NE	Sea	50	1572
75	Bos-Ed.	300	3200	5.0	ENE	Sea	50	1572
76	Bos-Ed.	300	3200	5.0	E	Sea	50	1572
77	Bos-Ed.	300	3200	5.0	ESE	Sea	50	1572
78	Bos-Ed.	300	3200	5.0	SE	Sea	50	1572
79	Bos-Ed.	300	3200	5.0	SSE	Land	50	1572
80	Bos-Ed.	300	3200	5.0	S	Land	50	1572
81	Bos-Ed.	300	3200	5.0	SSW	Land	50	1572
82	Bos-Ed.	300	3200	5.0	SW	Land	50	1572
83	Bos-Ed.	240	400	5.0	N	Land	50	196
84	Bos-Ed.	240	400	5.0	NNE	Sea	50	196
85	Bos-Ed.	240	400	5.0	E	Sea	50	196
86	Bos-Ed.	240	400	5.0	ESE	Sea	50	196
87	Bos-Ed.	240	400	5.0	SE	Sea	50	196
88	Bos-Ed.	240	400	5.0	SSE	Land	50	196
89	Bos-Ed.	240	400	5.0	S	Land	50	196
90	Bos-Ed.	240	400	5.0	SW	Land	50	196
91	Bos-Ed.	240	400	5.0	WSW	Land	50	196
92	Bos-Ed.	240	400	5.0	W	Land	50	196
93	Bos-Ed.	240	400	5.0	WNW	Land	50	196
94	Bos-Ed.	240	400	5.0	NW	Land	50	196
95	Bos-Ed.	240	400	5.0	NNW	Land	50	196
96	Bos-Ed.	240	800	5.0	N	Land	50	393
97	Bos-Ed.	240	800	5.0	NNE	Sea	50	393
98	Bos-Ed.	240	800	5.0	NE	Sea	50	393
99	Bos-Ed.	240	800	5.0	ENE	Sea	50	393
100	Bos-Ed.	240	800	5.0	E	Sea	50	393
101	Bos-Ed.	240	800	5.0	ESE	Sea	50	393
102	Bos-Ed.	240	800	5.0	SE	Sea	50	393
103	Bos-Ed.	240	800	5.0	SSE	Land	50	393
104	Bos-Ed.	240	800	5.0	S	Land	50	393
105	Bos-Ed.	240	800	5.0	SSW	Land	50	393
106	Bos-Ed.	240	800	5.0	SW	Land	50	393
107	Bos-Ed.	240	800	5.0	WSW	Land	50	393
108	Bos-Ed.	240	800	5.0	W	Land	50	393
109	Bos-Ed.	240	800	5.0	WNW	Land	50	393
110	Bos-Ed.	240	800	5.0	NW	Land	50	393
111	Bos-Ed.	240	800	5.0	NNW	Land	50	393
112	Bos-Ed.	240	1600	5.0	N	Land	50	786
113	Bos-Ed.	240	1600	5.0	NNE	Sea	50	786
114	Bos-Ed.	240	1600	5.0	E	Sea	50	786
115	Bos-Ed.	240	1600	5.0	ESE	Sea	50	786
116	Bos-Ed.	240	1600	5.0	SE	Sea	50	786
117	Bos-Ed.	240	1600	5.0	SSE	Land	50	786
118	Bos-Ed.	240	1600	5.0	S	Land	50	786
119	Bos-Ed.	240	1600	5.0	SW	Land	50	786
120	Bos-Ed.	240	1600	5.0	WSW	Land	50	786
121	Bos-Ed.	240	1600	5.0	W	Land	50	786
122	Bos-Ed.	240	1600	5.0	WNW	Land	50	786
123	Bos-Ed.	240	1600	5.0	NW	Land	50	786
124	Bos-Ed.	240	1600	5.0	NNW	Land	50	786
125	Bos-Ed.	240	3200	5.0	NNE	Sea	50	1572
126	Bos-Ed.	240	3200	5.0	NE	Sea	50	1572
127	Bos-Ed.	240	3200	5.0	ENE	Sea	50	1572
128	Bos-Ed.	240	3200	5.0	E	Sea	50	1572
129	Bos-Ed.	240	3200	5.0	ESE	Sea	50	1572
130	Bos-Ed.	240	3200	5.0	SE	Sea	50	1572
131	Bos-Ed.	240	3200	5.0	SSE	Land	50	1572
132	Bos-Ed.	240	3200	5.0	S	Land	50	1572
133	Bos-Ed.	240	3200	5.0	SSW	Land	50	1572
134	Bos-Ed.	240	3200	5.0	SW	Land	50	1572

Table 10 Concentration Results

Run No. = Point No.	Description	X (ft)	Y (Deg)	Z (ft)	1 K^	2 K^	3 K^	4 K^	5 K^	6 K^	7 K^	8 K^	9 K^	10 K^	11 K^	12 K^	13 K^	14 K^	15 K^
1	Sheraton Bldg (roof)	0	0	203					278	28					50	11	188	12	70
2	Harbor Towers (plume ht.)	1250	12	240					909	2560					776	2521			
3	Harbor Towers (pool)	1175	15	0					1701	250					751	202			
4	Boston Harbor Hotel	760	21	167					861	58					920	1436			
5	US Customs Bldg (Street)	390	22	0					5233	218					2267	22			
6	Rowe's Wharf	1075	31	89					5347	640					2284	231			
7	US Customs Bldg (roof)	450	32	140					9297	702					4843	135			
8	Northern Ave. & Sleeper St.	840	96	0															
9	Victoria Station Rest.	760	123	0															
10	Farnsworth Street	1250	135	0															
11	SE	1970	135	0															
12	Children's Museum	920	141	0															
13	Congress Street	1400	152	0															
14	Boston Tea Party Museum	640	172	0													21	0	
15	S (Necco St.)	1970	180	0													0	0	
16	Congress ST. & Dorchester Ave	710	200	0	45	0	2	2			11	0	2	0			155	28	0
17	Dorchester Ave. & Summer ST.	1025	202	0	107	4	10	4			56	6	6	0			185	70	0
18	Stone & Webster Bldg.	1140	213	226	1019	385	8	2			296	15	0	0			631	260	0
19	Fed Reserve intake # 3	920	230	538	176	136	1623	1031			227	240	1013	380			883	2064	529
20	Stearns Perry & Smith Co.	440	233	100	20876	96	1803	25			1805	20	169	9			1642	229	2486
21	South Station	1225	235	93	7787	1335	2128	401			4102	266	866	43			3398	1161	1847
22	Fed Reserve Intake # 2	960	236	98	16594	2646	1310	119			8505	256	265	2			5402	1998	1200
23	South Station (Street)	1200	240	0	7755	965	5926	631			3533	127	1962	47			3342	1133	2308
24	Dewey Square (roof)	1536	247	610	0	15	137	739			11	0	248	1553			10	10	233
25	Dewey Square (Street	1250	247	0	5597	405	8842	841			1741	48	3241	84			1471	473	1992
26	Fed Reserve (Street)	630	248	0	123	4	2155	50			30	0	391	1			46	17	893
27	Keystone Bldg (Intake)	775	269	192	0	1	6	1			0	1	0	0			8	0	1105
28	Keystone Bldg (Street)	780	269	0	0	6	0	0			3	0	0	0			8	0	200
29	Bldg betw High St. & Matthews	970	275	412			0	0					0	0			0	0	0
30	Western Union Bldg	640	277	187			0	0					0	0			0	0	193
31	Road House	600	281	40			0	0					0	0			29	2	121
32	125 High Street Bldg	630	294	226													3	6	0
33	New England T & T	1075	297	365															
34	New Fire House	450	307	24															
35	NW (Milk ST.)	1550	308	0															
36	State Street Bank Bldg.	900	315	443															
37	Oliver St. & Franklin St.	1125	320	0															
38	21 Story Tower	650	324	230															
39	Oliver St. & High St.	850	324	0															
40	Shops on Purchase & Olive	450	329	71					2	1					0	0			
41	Bldg on India & Milk (Roof)	1625	340	164					18	6					14	14			
42	International Place (Street)	510	348	0					5	2					3	8			
43	International Place (Intake)	600	350	42					0	0					0	0			
44	Bldg. on Broad & High (Roof)	975	353	82					5	7					5	5			
45	N (Atlantic Ave.)	1970	358	0					171	109					104	346			

note $K\hat{} = (\chi U/Q)*10^9$ $[ft^{-2}]$

Table 11 Concentration Results (continued)

Run No. = Point No.	Description	X (ft)	Y (Deg)	Z (ft)	16	17	18	19	20	21	22	23	24	25	26	27	28	29	30
					K^	K^	K^	K^	K^	K^	K^	K^	K^	K^	K^	K^	K^	K^	K^
1	Sheraton Bldg (roof)	0	0	203	0	0	12	8	6	5	4	0	0	29					34
2	Harbor Towers (plume ht.)	1250	12	240		4192	7764					7660	5745						3
3	Harbor Towers (pool)	1175	15	0		9367	416					4188	40						
4	Boston Harbor Hotel	760	21	167		16694	108					7394	21						
5	US Customs Bldg (Street)	390	22	0		4620	77					519	24						
6	Rowe's Wharf	1075	31	89		607	16					181	0						
7	US Customs Bldg (roof)	450	32	140		1629	42					101	13						
8	Northern Ave. & Sleeper St.	840	96	0										0					
9	Victoria Station Rest.	760	123	0										0					
10	Farnsworth Street	1250	135	0										0					
11	SE	1970	135	0										0					
12	Children's Museum	920	141	0										0	18				
13	Congress Street	1400	152	0										2	32				
14	Boston Tea Party Museum	640	172	0				2	2					24	51	19	16		
15	S (Necco St.)	1970	180	0				8	0					1022	10	2	2		
16	Congress ST. & Dorchester Ave	710	200	0	0			24	0	30	0			1227	113	24	14	24	
17	Dorchester Ave. & Summer ST.	1025	202	0	0			30	3	0	1			2117	1826	51	24	27	
18	Stone & Webster Bldg.	1140	213	226	0			227	16	0	0			583	9751	227	16	0	
19	Fed Reserve intake # 3	920	230	538	266			1631	6159	441	186			0	5	296	720	29	14
20	Stearns Perry & Smith Co.	440	233	100	238			321	25	399	14			45	1067	1787	371	18	5
21	South Station	1225	235	93	371			1784	466	703	71			6	1765	4340	863	26	8
22	Fed Reserve Intake # 2	960	236	98	232			3270	647	335	38			38	855	8358	152	16	10
23	South Station (Street)	1200	240	0	508			1751	383	732	56			0	1743	3177	1821	73	89
24	Dewey Square (roof)	1536	247	610	1345			46	58	615	2721			0	53	10	257	0	
25	Dewey Square (Street	1250	247	0	417			744	115	756	57			0	316	1526	2902	677	447
26	Fed Reserve (Street)	630	248	0	29			6	0	94	2			0	16	18	682	933	454
27	Keystone Bldg (Intake)	775	269	192	272			8	0	754	23				37	5	6	1065	3578
28	Keystone Bldg (Street)	780	269	0	4			2	0	35	4				158	34	5	70	580
29	Bldg betw High St. & Matthews	970	275	412				0	0	10	0				8	2	3	292	4714
30	Western Union Bldg	640	277	187				2	0	112	1				11	6	5	24	6815
31	Road House	600	281	40				8	0	34	0				30	27	6	21	335
32	125 High Street Bldg	630	294	226				0	0	3	1				13	6	10	18	155
33	New England T & T	1075	297	365													8	0	1794
34	New Fire House	450	307	24														16	10
35	NW (Milk ST.)	1550	308	0														0	5979
36	State Street Bank Bldg.	900	315	443														0	35
37	Oliver St. & Franklin St.	1125	320	0														96	2355
38	21 Story Tower	650	324	230														0	10
39	Oliver St. & High St.	850	324	0														0	3
40	Shops on Purchase & Olive	450	329	71		0	0					3	0						3
41	Bldg on India & Milk (Roof)	1625	340	164		482	11					153	0						0
42	International Place (Street)	510	348	0		0	1					0	0						5
43	International Place (Intake)	600	350	42		0	0					0	0						0
44	Bldg. on Broad & High (Roof)	975	353	82		272	1					86	0						2
45	N (Atlantic Ave.)	1970	358	0		2450	524					1259	228						11

note K^ = $(\chi U/Q)*10^9$ $[ft^{-2}]$

Table 12 Concentration Results (continued)

Run No. = Point No.	Description	X (ft)	Y (Deg)	Z (ft)	31 K^	32 K^	33 K^	34 K^	35 K^	36 K^	37 K^	38 K^	39 K^	40 K^	41 K^	42 K^	43 K^	44 K^	45 K^
1	Sheraton Bldg (roof)	0	0	203	2	19	163	193	267	2040	1355	78	54	35	15				
2	Harbor Towers (plume ht.)	1250	12	240	0	0	2538	1816	19	5	0								
3	Harbor Towers (pool)	1175	15	0	0	24	1310	580	113	18	0								
4	Boston Harbor Hotel	760	21	167	0	5	1292	1252	131	48	0								
5	US Customs Bldg (Street)	390	22	0	2	0	67	1748	305	70	21	59							
6	Rowe's Wharf	1075	31	89	0	0	18	1907	1361	273	137	0							
7	US Customs Bldg (roof)	450	32	140	2	13	275	3307	903	165	19	16							
8	Northern Ave. & Sleeper St.	840	96	0				80	86	54	2610	377	10	0	4				
9	Victoria Station Rest.	760	123	0					35	11	109	361	45	0	5				
10	Farnsworth Street	1250	135	0						0	0	149	1136	19	4				
11	SE	1970	135	0						11	0	27	1602	21	4				
12	Children's Museum	920	141	0						8	0	120	748	11	6	1			
13	Congress Street	1400	152	0							0	24	2182	395	9	7			
14	Boston Tea Party Museum	640	172	0							0	10	1589	1310	26	11	10	7	
15	S (Necco St.)	1970	180	0								0	8	1712	1211	0	0	0	
16	Congress ST. & Dorchester Ave	710	200	0								0	494	4017	517	16	8	6	2
17	Dorchester Ave. & Summer ST.	1025	202	0									19	1192	581	1012	22	13	3
18	Stone & Webster Bldg.	1140	213	226										105	181	3268	228	7	0
19	Fed Reserve intake # 3	920	230	538	0									0	3	5	351	548	6
20	Stearns Perry & Smith Co.	440	233	100	11	0								62	6	114	192	59	0
21	South Station	1225	235	93	2	0									4	546	1340	317	6
22	Fed Reserve Intake # 2	960	236	98	0	0									13	153	1919	84	2
23	South Station (Street)	1200	240	0	3	3									3	442	720	647	15
24	Dewey Square (roof)	1536	247	610										0	3	13	0	717	0
25	Dewey Square (Street	1250	247	0	21	2									3	112	373	954	97
26	Fed Reserve (Street)	630	248	0	101	0									3	6	13	115	103
27	Keystone Bldg (Intake)	775	269	192	59	0										15	2	1	1533
28	Keystone Bldg (Street)	780	269	0	1150	0										61	38	1	9
29	Bldg betw High St. & Matthews	970	275	412	97	0										3	0	0	409
30	Western Union Bldg	640	277	187	1165	0	11									10	4	2	1
31	Road House	600	281	40	2958	0	16									18	12	2	1
32	125 High Street Bldg	630	294	226	7364	35	14									25	7	5	1
33	New England T & T	1075	297	365	4655	0	5											2	1
34	New Fire House	450	307	24	45	129	24	19	26	13									0
35	NW (Milk ST.)	1550	308	0	2233	171	18	10	6	5									1
36	State Street Bank Bldg.	900	315	443	3300	1478	19	10	5	3									0
37	Oliver St. & Franklin St.	1125	320	0	1257	161	13	13	11	6									116
38	21 Story Tower	650	324	230	6	5474	65	14	10	5									0
39	Oliver St. & High St.	850	324	0	1193	1088	43	21	27	5									0
40	Shops on Purchase & Olive	450	329	71	5	1696	27	14	14	10									
41	Bldg on India & Milk (Roof)	1625	340	164	16	2310	267	30	11										
42	International Place (Street)	510	348	0	2	669	35	22	27	18									
43	International Place (Intake)	600	350	42	0	1006	125	18	24	18									
44	Bldg. on Broad & High (Roof)	975	353	82	0	538	922	35	21	10									
45	N (Atlantic Ave.)	1970	358	0	0	61	2917	147	26	8									

note K^ = $(\chi U/Q)*10^9$ $[ft^{-2}]$

Table 13 Concentration Results (continued)

Point No.	Description	X (ft)	Y (Deg)	Z (ft)	Run No. = 46 K^	47 K^	48 K^	49 K^	50 K^	51 K^	52 K^	53 K^	54 K^	55 K^	56 K^	57 K^	58 K^	59 K^	60 K^
1	Sheraton Bldg (roof)	0	0	203	38	11	22	25	19	22	269	425	87	34	12	13			
2	Harbor Towers (plume ht.)	1250	12	240		0	2	1776	1954	8	0	0							
3	Harbor Towers (pool)	1175	15	0		0	15	565	376	31	10	0							
4	Boston Harbor Hotel	760	21	167		0	8	603	814	42	24	9							
5	US Customs Bldg (Street)	390	22	0		0	3	18	269	25	23	28	64						
6	Rowe's Wharf	1075	31	89		0	3	1	801	598	152	129	10						
7	US Customs Bldg (roof)	450	32	140		12	22	58	1015	166	106	91	50						
8	Northern Ave. & Sleeper St.	840	96	0					14	10	48	1554	181	6	1	2			
9	Victoria Station Rest.	760	123	0						4	10	173	385	44	0	3			
10	Farnsworth Street	1250	135	0							0	0	208	989	33	3			
11	SE	1970	135	0							5	0	78	1506	40	1			
12	Children's Museum	920	141	0							9	0	184	480	25	2	2		
13	Congress Street	1400	152	0								0	77	1775	406	6	3		
14	Boston Tea Party Museum	640	172	0								22	52	1129	639	15	4	6	8
15	S (Necco St.)	1970	180	0									0	4	1060	921	1	4	6
16	Congress ST. & Dorchester Ave	710	200	0									13	246	1688	142	11	5	7
17	Dorchester Ave. & Summer ST.	1025	202	0										6	342	202	151	8	10
18	Stone & Webster Bldg.	1140	213	226											17	37	733	52	6
19	Fed Reserve intake # 3	920	230	538	8	2									0	0	0	614	509
20	Stearns Perry & Smith Co.	440	233	100	4	0	2								47	3	27	34	13
21	South Station	1225	235	93	6	0	2									1	73	122	27
22	Fed Reserve Intake # 2	960	236	98	9	0	2									16	14	121	8
23	South Station (Street)	1200	240	0	38	5	8									0	68	60	42
24	Dewey Square (roof)	1536	247	610	2										0	0	2	1	2831
25	Dewey Square (Street	1250	247	0	93	7	3									0	18	23	60
26	Fed Reserve (Street)	630	248	0	73	25	0									0	1	2	9
27	Keystone Bldg (Intake)	775	269	192	599	7	2										5	2	3
28	Keystone Bldg (Street)	780	269	0	363	354	0										20	13	3
29	Bldg betw High St. & Matthews	970	275	412	2444	24	1										0	0	2
30	Western Union Bldg	640	277	187	4483	234	0	0									3	3	4
31	Road House	600	281	40	231	832	0	0									5	6	4
32	125 High Street Bldg	630	294	226	203	3190	11	0									9	4	6
33	New England T & T	1075	297	365	3900	1976	2	0											4
34	New Fire House	450	307	24	16	24	26	0	0	0	12								
35	NW (Milk ST.)	1550	308	0	3405	771	116	1	0	0	0								
36	State Street Bank Bldg.	900	315	443	44	4898	1498	7	0	0	0								
37	Oliver St. & Franklin St.	1125	320	0	1358	412	101	0	0	0	9								
38	21 Story Tower	650	324	230	6	15	3518	27	1	0	2								
39	Oliver St. & High St.	850	324	0	6	492	614	11	0	0	2								
40	Shops on Purchase & Olive	450	329	71	3	6	732	3	0	0	6								
41	Bldg on India & Milk (Roof)	1625	340	164	1	5	2142	330	9	2									
42	International Place (Street)	510	348	0	4	0	475	5	0	0	18								
43	International Place (Intake)	600	350	42	0	0	962	64	0	1	133								
44	Bldg. on Broad & High (Roof)	975	353	82	1	0	515	1188	16	2	4								
45	N (Atlantic Ave.)	1970	358	0	11	0	42	2748	120	6	2								

note $K^{\wedge} = (\chi U/Q) \cdot 10^9$ [ft^{-2}]

Table 14 Concentration Results (continued)

Run No. = Point No.	Description	X (ft)	Y (Deg)	Z (ft)	61 K^	62 K^	63 K^	64 K^	65 K^	66 K^	67 K^	68 K^	69 K^	70 K^	71 K^	72 K^	73 K^	74 K^	75 K^
1	Sheraton Bldg (roof)	0	0	203		32	29	10	17	17	31	122	175	95	44	40			
2	Harbor Towers (plume ht.)	1250	12	240			0	0	470	2758	16	2	2						
3	Harbor Towers (pool)	1175	15	0			4	0	70	128	14	5	1						
4	Boston Harbor Hotel	760	21	167			6	0	53	249	13	10	10						
5	US Customs Bldg (Street)	390	22	0			7	0	2	20	24	10	17	54					
6	Rowe's Wharf	1075	31	89			5	0	0	101	312	40	55	7					
7	US Customs Bldg (roof)	450	32	140			32	9	25	101	127	50	54	64					
8	Northern Ave. & Sleeper St.	840	96	0						10	18	24	503	223	10	8			
9	Victoria Station Rest.	760	123	0							5	2	36	232	34	5			
10	Farnsworth Street	1250	135	0								0	0	213	623	16			
11	SE	1970	135	0								0	0	28	1016	34			
12	Children's Museum	920	141	0								2	13	112	369	9	1		
13	Congress Street	1400	152	0									0	16	1051	201	4		
14	Boston Tea Party Museum	640	172	0									12	19	479	137	5	12	10
15	S (Necco St.)	1970	180	0										2	0	585	0	1	0
16	Congress ST. & Dorchester Ave	710	200	0	6									5	91	383	1	9	8
17	Dorchester Ave. & Summer ST.	1025	202	0	6										6	109	14	13	14
18	Stone & Webster Bldg.	1140	213	226	4											8	93	9	3
19	Fed Reserve intake # 3	920	230	538	8	8	10									0	0	826	180
20	Stearns Perry & Smith Co.	440	233	100	4	5	7	0								11	25	128	22
21	South Station	1225	235	93	6	6	7	2									13	19	8
22	Fed Reserve Intake # 2	960	236	98	5	8	8	1									3	24	2
23	South Station (Street)	1200	240	0	10	25	14	4									19	19	15
24	Dewey Square (roof)	1536	247	610	16	4										0	0	0	3033
25	Dewey Square (Street	1250	247	0	14	23	14	2									11	19	22
26	Fed Reserve (Street)	630	248	0	9	11	14	1									0	3	11
27	Keystone Bldg (Intake)	775	269	192	289	159	6	1									4	1	0
28	Keystone Bldg (Street)	780	269	0	4	41	64	0									26	28	0
29	Bldg betw High St. & Matthews	970	275	412	477	1270	14	1									0	0	0
30	Western Union Bldg	640	277	187	3	694	45	0	1								0	1	0
31	Road House	600	281	40	2	31	176	0	2								3	8	4
32	125 High Street Bldg	630	294	226	2	172	589	1	2								0	2	2
33	New England T & T	1075	297	365	2	4687	591	1	1										0
34	New Fire House	450	307	24	2	22	8	4	3	3	6	8							
35	NW (Milk ST.)	1550	308	0	0	1191	186	65	3	1	2	2							
36	State Street Bank Bldg.	900	315	443	1	36	3379	1617	11	3	2	2							
37	Oliver St. & Franklin St.	1125	320	0	101	496	80	22	2	2	3	4							
38	21 Story Tower	650	324	230	0	3	4	690	40	2	2	1							
39	Oliver St. & High St.	850	324	0	0	2	109	153	10	4	5	3							
40	Shops on Purchase & Olive	450	329	71		4	6	104	3	3	4	5							
41	Bldg on India & Milk (Roof)	1625	340	164		0	4	1131	470	9	4								
42	International Place (Street)	510	348	0		4	7	48	6	6	8	12							
43	International Place (Intake)	600	350	42		0	3	85	16	2	6	8							
44	Bldg. on Broad & High (Roof)	975	353	82		0	2	74	512	7	5	4							
45	N (Atlantic Ave.)	1970	358	0		3	1	5	1115	87	5	3							

note K^ = $(\chi U/Q)*10^9$ $[ft^{-2}]$

Table 15 Concentration Results (continued)

Run No. = Point No.	Description	X (ft)	Y (Deg)	Z (ft)	76 K^	77 K^	78 K^	79 K^	80 K^	81 K^	82 K^	83 K^	84 K^	85 K^	86 K^	87 K^	88 K^	89 K^	90 K^
1	Sheraton Bldg (roof)	0	0	203		14	33	15	21	25	42	8			11	22	24	18	973
2	Harbor Towers (plume ht.)	1250	12	240			1	0	146	1090	8					0	2	2062	37
3	Harbor Towers (pool)	1175	15	0			6	0	13	19	9					0	67	970	244
4	Boston Harbor Hotel	760	21	167			9	0	10	22	15					2	38	800	371
5	US Customs Bldg (Street)	390	22	0			8	0	2	6	10					2	2	107	636
6	Rowe's Wharf	1075	31	89			7	0	1	16	52					0	2	16	2645
7	US Customs Bldg (roof)	450	32	140			31	14	28	31	41					0	3	299	4907
8	Northern Ave. & Sleeper St.	840	96	0						19	27	0							11
9	Victoria Station Rest.	760	123	0							9	0							3
10	Farnsworth Street	1250	135	0								0							
11	SE	1970	135	0								0							
12	Children's Museum	920	141	0								0	0						
13	Congress Street	1400	152	0								0	0						
14	Boston Tea Party Museum	640	172	0								10	0						
15	S (Necco St.)	1970	180	0								540	0						
16	Congress ST. & Dorchester Ave	710	200	0	7							1080	139	0					
17	Dorchester Ave. & Summer ST.	1025	202	0	8							1962	2535	0					
18	Stone & Webster Bldg.	1140	213	226	0							380	7608	0					
19	Fed Reserve intake # 3	920	230	538	4	3	7					0	2	6	3	3			
20	Stearns Perry & Smith Co.	440	233	100	1	4	6	0				51	826	37	0	0	0		
21	South Station	1225	235	93	6	3	4	0				0	1725	0	0	0	0		
22	Fed Reserve Intake # 2	960	236	98	1	3	5	0				35	466	0	0	0	0		
23	South Station (Street)	1200	240	0	19	9	13	0				0	1361	0	5	0	2		
24	Dewey Square (roof)	1536	247	610	4	2						0	30	0	0				
25	Dewey Square (Street	1250	247	0	17	8	12	0				0	331	465	203	0	3		
26	Fed Reserve (Street)	630	248	0	13	6	9	0				0	19	7979	887	276	3		
27	Keystone Bldg (Intake)	775	269	192	13	23	2	0					11	5457	463	19	2		
28	Keystone Bldg (Street)	780	269	0	5	4	20	0					10	1660	3938	388	2		
29	Bldg betw High St. & Matthews	970	275	412	191	184	3	0					6	1672	1915	21	2		
30	Western Union Bldg	640	277	187	0	18	10	0	0				32	434	18801	438	3	0	
31	Road House	600	281	40	3	3	24	0	1				21	160	2324	2160	5	0	
32	125 High Street Bldg	630	294	226	1	62	53	0	1				46	51	767	5255	3	2	
33	New England T & T	1075	297	365	0	1484	96	0	0					56	4056	922	3	2	
34	New Fire House	450	307	24	2	8	6	0	3	5	10			5	18	208	131	6	0
35	NW (Milk ST.)	1550	308	0	0	227	33	3	2	1	2			58	8060	1529	80	2	3
36	State Street Bank Bldg.	900	315	443	0	8	1244	742	5	2	2			19	105	11878	211	3	6
37	Oliver St. & Franklin St.	1125	320	0	47	44	13	0	1	3	5			3	32	2088	412	5	0
38	21 Story Tower	650	324	230	0	1	3	52	13	2	2			2	2	818	10108	133	11
39	Oliver St. & High St.	850	324	0	0	1	21	18	3	5	8			3	5	1872	1548	24	3
40	Shops on Purchase & Olive	450	329	71		3	6	1	3	4	6				2	228	2244	18	8
41	Bldg on India & Milk (Roof)	1625	340	164		2	3	429	315	5	3				0	46	3709	227	43
42	International Place (Street)	510	348	0		5	8	4	8	9	13				0	14	2201	24	2
43	International Place (Intake)	600	350	42		0	3	1	5	4	9				0	5	4655	235	14
44	Bldg. on Broad & High (Roof)	975	353	82		1	2	0	125	5	6				0	5	2174	1329	19
45	N (Atlantic Ave.)	1970	358	0		5	4	0	380	38	5				0	0	232	4203	45

note K^ = $(\chi U/Q) * 10^9$ $[ft^{-2}]$

Table 16 Concentration Results (continued)

Run No. = Point No.	Description	X (ft)	Y (Deg)	Z (ft)	91 K^	92 K^	93 K^	94 K^	95 K^	96 K^	97 K^	98 K^	99 K^	100 K^	101 K^	102 K^	103 K^	104 K^	105 K^
1	Sheraton Bldg (roof)	0	0	203	1551	1371	283	88	35	18					10	14	0	34	123
2	Harbor Towers (plume ht.)	1250	12	240	3	0										0	0	2949	2018
3	Harbor Towers (pool)	1175	15	0	13	0										0	65	1082	465
4	Boston Harbor Hotel	760	21	167	45	3										0	54	871	1005
5	US Customs Bldg (Street)	390	22	0	169	104	58									0	0	133	711
6	Rowe's Wharf	1075	31	89	358	366	2									0	0	25	3216
7	US Customs Bldg (roof)	450	32	140	332	104	8									0	0	405	7385
8	Northern Ave. & Sleeper St.	840	96	0	10	2107	254	0	0	2									4
9	Victoria Station Rest.	760	123	0	0	220	550	22	0	3									
10	Farnsworth Street	1250	135	0	0	16	414	1351	0	2									
11	SE	1970	135	0	0	8	72	1669	0	2									
12	Children's Museum	920	141	0	2	8	289	1351	0	2	0								
13	Congress Street	1400	152	0		3	53	3502	264	3	0								
14	Boston Tea Party Museum	640	172	0		54	64	3910	2821	17	0	0	0						
15	S (Necco St.)	1970	180	0			11	46	2272	998	0	0	0						
16	Congress ST. & Dorchester Ave	710	200	0			16	1184	9174	601	49	1	0	0					
17	Dorchester Ave. & Summer ST.	1025	202	0				6	2759	850	788	5	0	0					
18	Stone & Webster Bldg.	1140	213	226					152	142	3065	141	1	0					
19	Fed Reserve intake # 3	920	230	538					0	2	2	568	815	1	2	2			
20	Stearns Perry & Smith Co.	440	233	100					240	12	121	1641	815	10	0	0	0		
21	South Station	1225	235	93						10	458	4563	434	0	0	0	0		
22	Fed Reserve Intake # 2	960	236	98						40	67	7530	499	0	0	0	0		
23	South Station (Street)	1200	240	0						31	373	3073	1424	1	3	0	0		
24	Dewey Square (roof)	1536	247	610					0	2	10	2	215	0	1				
25	Dewey Square (Street	1250	247	0						2	37	2121	3855	165	52	0	0		
26	Fed Reserve (Street)	630	248	0						16	4	46	823	1581	324	146	0		
27	Keystone Bldg (Intake)	775	269	192							38	10	11	9936	195	3	0		
28	Keystone Bldg (Street)	780	269	0							2	0	1	201	2642	762	0		
29	Bldg betw High St. & Matthews	970	275	412							26	7	6	2611	1022	12	0		
30	Western Union Bldg	640	277	187							6	2	2	176	13473	518	0	2	
31	Road House	600	281	40							2	2	2	31	1860	2699	0	2	
32	125 High Street Bldg	630	294	226							5	2	2	20	1007	5428	0	2	
33	New England T & T	1075	297	365									7	68	5324	1007	0	2	
34	New Fire House	450	307	24	3									2	19	204	76	3	1
35	NW (Milk ST.)	1550	308	0	2									82	6254	1590	52	2	0
36	State Street Bank Bldg.	900	315	443	3									18	174	9613	289	9	2
37	Oliver St. & Franklin St.	1125	320	0	3									4	44	1910	228	5	1
38	21 Story Tower	650	324	230	8									2	5	411	6876	39	8
39	Oliver St. & High St.	850	324	0	5									4	22	1667	1224	11	2
40	Shops on Purchase & Olive	450	329	71	3										2	157	1221	11	2
41	Bldg on India & Milk (Roof)	1625	340	164											2	36	3354	185	8
42	International Place (Street)	510	348	0	6										3	4	1383	14	3
43	International Place (Intake)	600	350	42	21										1	2	3643	71	3
44	Bldg. on Broad & High (Roof)	975	353	82	13										1	2	2013	688	6
45	N (Atlantic Ave.)	1970	358	0	5										3	0	152	3787	104

note $K\hat{} = (\chi U/Q) * 10^9$ $[ft^{-2}]$

Table 17 Concentration Results (continued)

Run No. = Point No.	Description	X (ft)	Y (Deg)	Z (ft)	106 K^	107 K^	108 K^	109 K^	110 K^	111 K^	112 K^	113 K^	114 K^	115 K^	116 K^	117 K^	118 K^	119 K^	120 K^
1	Sheraton Bldg (roof)	0	0	203	77	298	609	68	11	14	12			11	17	17	43	29	73
2	Harbor Towers (plume ht.)	1250	12	240	22	3	2								0	0	1593	0	0
3	Harbor Towers (pool)	1175	15	0	153	10	2								0	52	322	6	3
4	Boston Harbor Hotel	760	21	167	206	21	2								1	46	96	51	7
5	US Customs Bldg (Street)	390	22	0	280	62	102	42							1	0	30	71	18
6	Rowe's Wharf	1075	31	89	1490	222	206	4							0	0	9	334	61
7	US Customs Bldg (roof)	450	32	140	1712	211	62	5							0	0	50	538	59
8	Northern Ave. & Sleeper St.	840	96	0	3	8	1720	170	3	3	0							10	6
9	Victoria Station Rest.	760	123	0	2	2	237	518	41	3	0							0	1
10	Farnsworth Street	1250	135	0		2	2	323	926	9	0								0
11	SE	1970	135	0		2	2	120	1349	11	0								2
12	Children's Museum	920	141	0		2	2	402	916	7	0	0							1
13	Congress Street	1400	152	0			2	66	2325	133	0	0							
14	Boston Tea Party Museum	640	172	0			3	143	1599	1520	0	2							
15	S (Necco St.)	1970	180	0				9	10	1733	536	0							
16	Congress ST. & Dorchester Ave	710	200	0				14	504	4208	146	0	0						
17	Dorchester Ave. & Summer ST.	1025	202	0					5	1039	258	106	0						
18	Stone & Webster Bldg.	1140	213	226						81	36	855	0						
19	Fed Reserve intake # 3	920	230	538						1	0	0	0	0	0				
20	Stearns Perry & Smith Co.	440	233	100						79	0	20	7	0	0	0			
21	South Station	1225	235	93							0	121	0	0	0	0			
22	Fed Reserve Intake # 2	960	236	98							4	25	0	0	0	0			
23	South Station (Street)	1200	240	0							0	108	6	0	0	0			
24	Dewey Square (roof)	1536	247	610						2	0	1	0	0					
25	Dewey Square (Street	1250	247	0							0	9	15	5	0	0			
26	Fed Reserve (Street)	630	248	0							0	0	68	33	31	0			
27	Keystone Bldg (Intake)	775	269	192								0	3755	84	7	0			
28	Keystone Bldg (Street)	780	269	0								0	28	482	98	0			
29	Bldg betw High St. & Matthews	970	275	412								0	2214	289	10	0			
30	Western Union Bldg	640	277	187								0	16	3293	96	0	0		
31	Road House	600	281	40								0	5	448	432	0	0		
32	125 High Street Bldg	630	294	226								0	9	1077	950	0	0		
33	New England T & T	1075	297	365									23	7994	260	0	0		
34	New Fire House	450	307	24	1	2							1	25	46	0	0	1	0
35	NW (Milk ST.)	1550	308	0	2	2							12	2123	403	39	0	0	0
36	State Street Bank Bldg.	900	315	443	2	2							60	66	8395	649	0	0	0
37	Oliver St. & Franklin St.	1125	320	0	1	2							4	9	495	102	0	0	0
38	21 Story Tower	650	324	230	5	4							1	0	74	3254	11	0	2
39	Oliver St. & High St.	850	324	0	2	2							4	2	400	427	0	0	0
40	Shops on Purchase & Olive	450	329	71	18	3								1	28	326	0	0	1
41	Bldg on India & Milk (Roof)	1625	340	164	4									0	8	2078	149	0	
42	International Place (Street)	510	348	0	2	3								1	4	359	0	0	2
43	International Place (Intake)	600	350	42	2	6								0	0	1271	47	0	1
44	Bldg. on Broad & High (Roof)	975	353	82	6	5								0	0	573	551	0	1
45	N (Atlantic Ave.)	1970	358	0	16	5								2	0	71	3377	14	2

note K^ = $(\chi U/Q)*10^9$ $[ft^{-2}]$

Table 18 Concentration Results (continued)

Run No. = Point No.	Description	X (ft)	Y (Deg)	Z (ft)	121 K^	122 K^	123 K^	124 K^	125 K^	126 K^	127 K^	128 K^	129 K^	130 K^	131 K^	132 K^	133 K^	134 K^
1	Sheraton Bldg (roof)	0	0	203	283	21	21	15					8	3	8	10	9	13
2	Harbor Towers (plume ht.)	1250	12	240	0									0	0	745	1207	6
3	Harbor Towers (pool)	1175	15	0	0									0	45	127	35	4
4	Boston Harbor Hotel	760	21	167	0									0	26	36	132	12
5	US Customs Bldg (Street)	390	22	0	62	80								0	0	0	27	3
6	Rowe's Wharf	1075	31	89	90	0								0	0	0	209	120
7	US Customs Bldg (roof)	450	32	140	17	17								0	0	6	392	62
8	Northern Ave. & Sleeper St.	840	96	0	753	278	0	0									1	2
9	Victoria Station Rest.	760	123	0	58	474	52	0										0
10	Farnsworth Street	1250	135	0	0	479	1041	5										
11	SE	1970	135	0	0	60	1194	6										
12	Children's Museum	920	141	0	0	334	852	3	0									
13	Congress Street	1400	152	0	0	58	1568	92	0									
14	Boston Tea Party Museum	640	172	0	0	35	841	222	1	1	0							
15	S (Necco St.)	1970	180	0		0	4	735	0	0	0							
16	Congress ST. & Dorchester Ave	710	200	0		0	221	1545	1	2	0	0						
17	Dorchester Ave. & Summer ST.	1025	202	0			5	562	13	3	0	0						
18	Stone & Webster Bldg.	1140	213	226				32	106	1	0	0						
19	Fed Reserve intake # 3	920	230	538				0	17	3401	1948	0	3	0				
20	Stearns Perry & Smith Co.	440	233	100				10	4	21	44	12	4	0	0			
21	South Station	1225	235	93					10	68	13	0	3	0	0			
22	Fed Reserve Intake # 2	960	236	98					2	110	12	0	3	0	0			
23	South Station (Street)	1200	240	0					10	34	24	0	4	0	0			
24	Dewey Square (roof)	1536	247	610				0	5	24	4862	0	4					
25	Dewey Square (Street	1250	247	0					2	18	50	2	5	0	0			
26	Fed Reserve (Street)	630	248	0					2	4	9	9	7	11	0			
27	Keystone Bldg (Intake)	775	269	192					1	2	3	813	62	0	0			
28	Keystone Bldg (Street)	780	269	0					1	1	0	4	33	56	0			
29	Bldg betw High St. & Matthews	970	275	412					1	3	6	1219	270	0	0			
30	Western Union Bldg	640	277	187					1	2	0	7	479	43	0	0		
31	Road House	600	281	40					1	2	0	0	20	160	0	0		
32	125 High Street Bldg	630	294	226					1	2	0	3	530	322	0	0		
33	New England T & T	1075	297	365							8	40	5071	114	0	0		
34	New Fire House	450	307	24								0	19	4	0	0	0	0
35	NW (Milk ST.)	1550	308	0								7	889	131	2	0	0	0
36	State Street Bank Bldg.	900	315	443								2	77	4289	79	0	0	0
37	Oliver St. & Franklin St.	1125	320	0								0	9	130	15	0	1	0
38	21 Story Tower	650	324	230								0	4	7	974	57	2	0
39	Oliver St. & High St.	850	324	0								0	6	101	73	3	0	0
40	Shops on Purchase & Olive	450	329	71									4	0	27	0	0	0
41	Bldg on India & Milk (Roof)	1625	340	164									4	2	1332	208	4	0
42	International Place (Street)	510	348	0									4	0	46	8	1	1
43	International Place (Intake)	600	350	42									4	0	434	99	1	0
44	Bldg. on Broad & High (Roof)	975	353	82									4	0	190	412	4	1
45	N (Atlantic Ave.)	1970	358	0									5	0	40	1804	41	6

note K^ = $(\chi U/Q)*10^9$ $[ft^{-2}]$

FIGURES

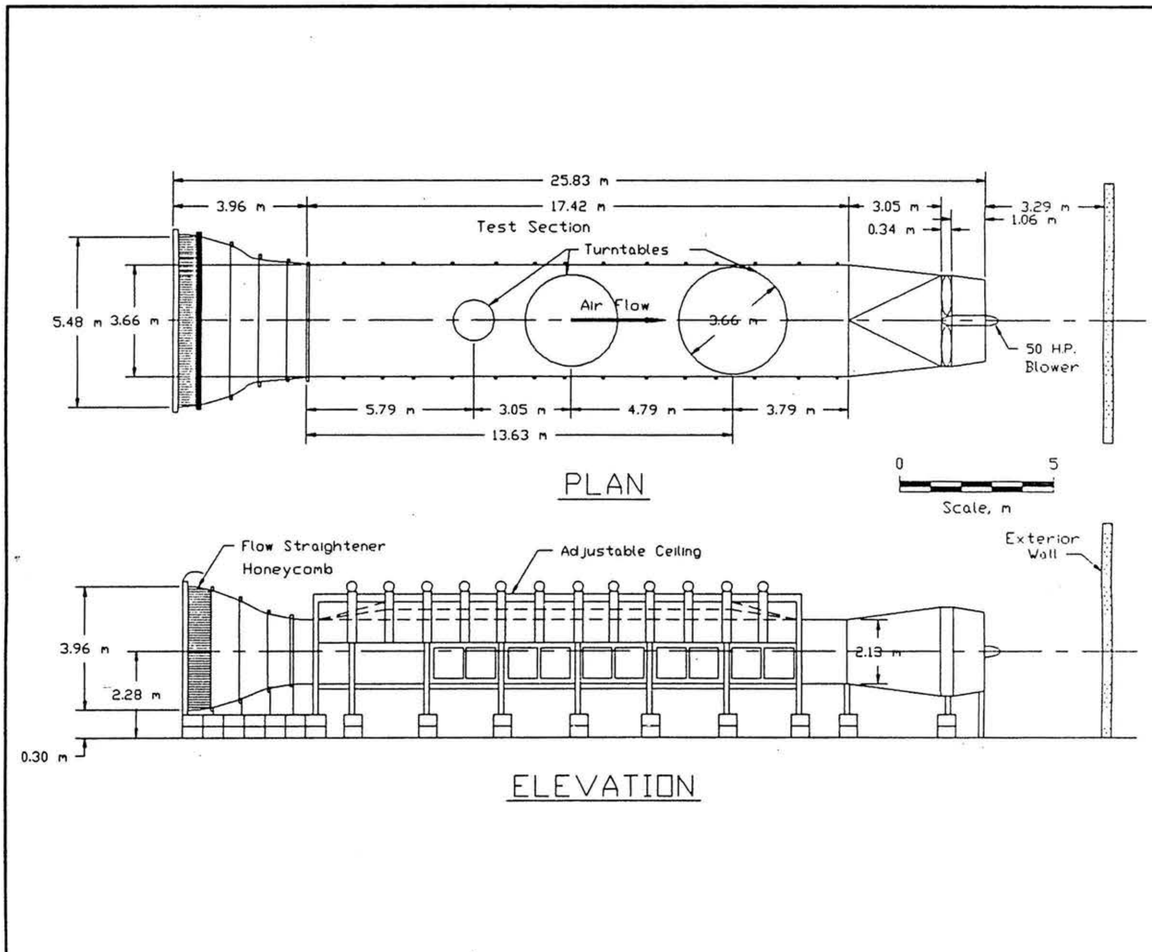

Figure 1 Environmental Wind Tunnel

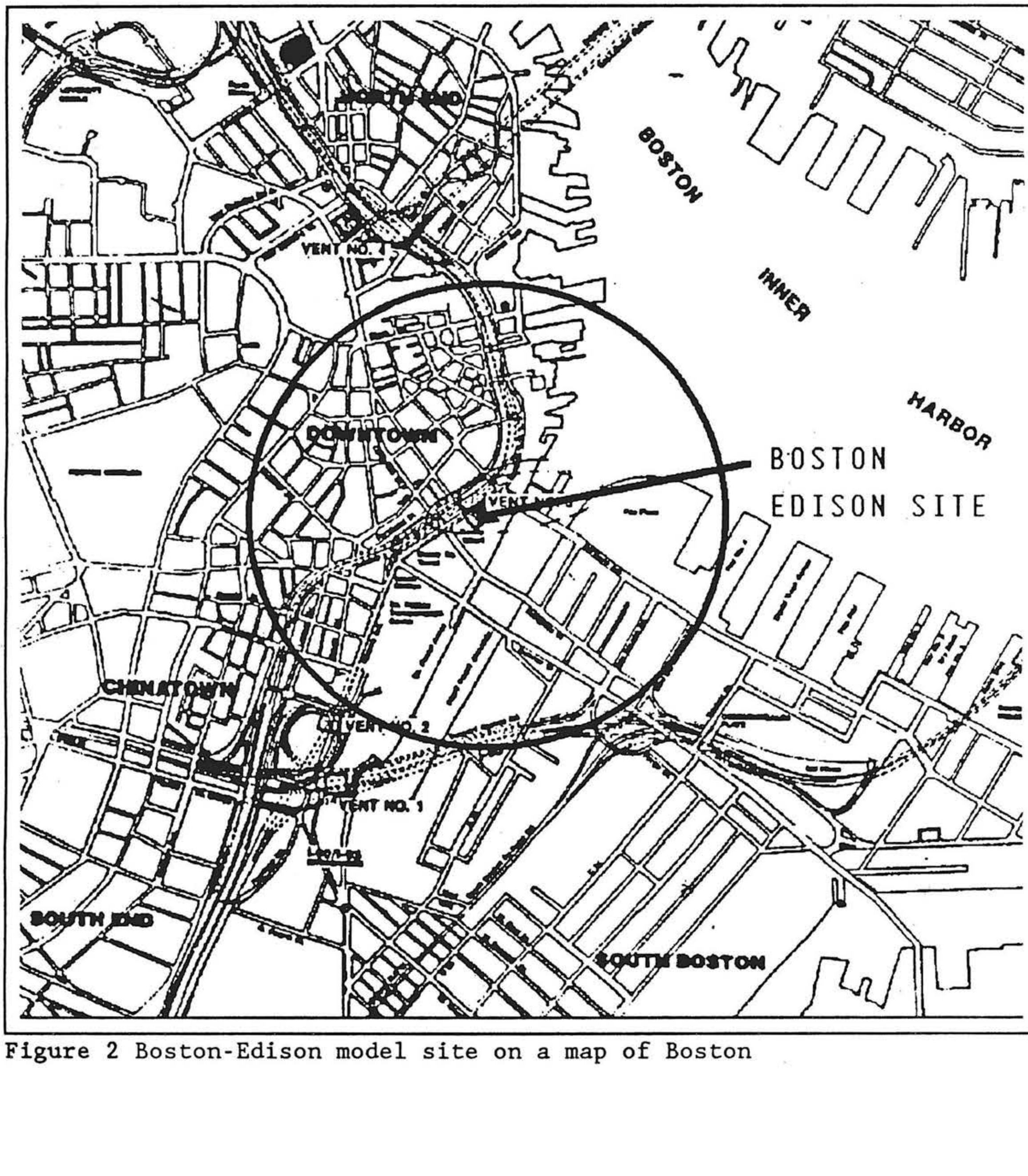

Figure 2 Boston-Edison model site on a map of Boston

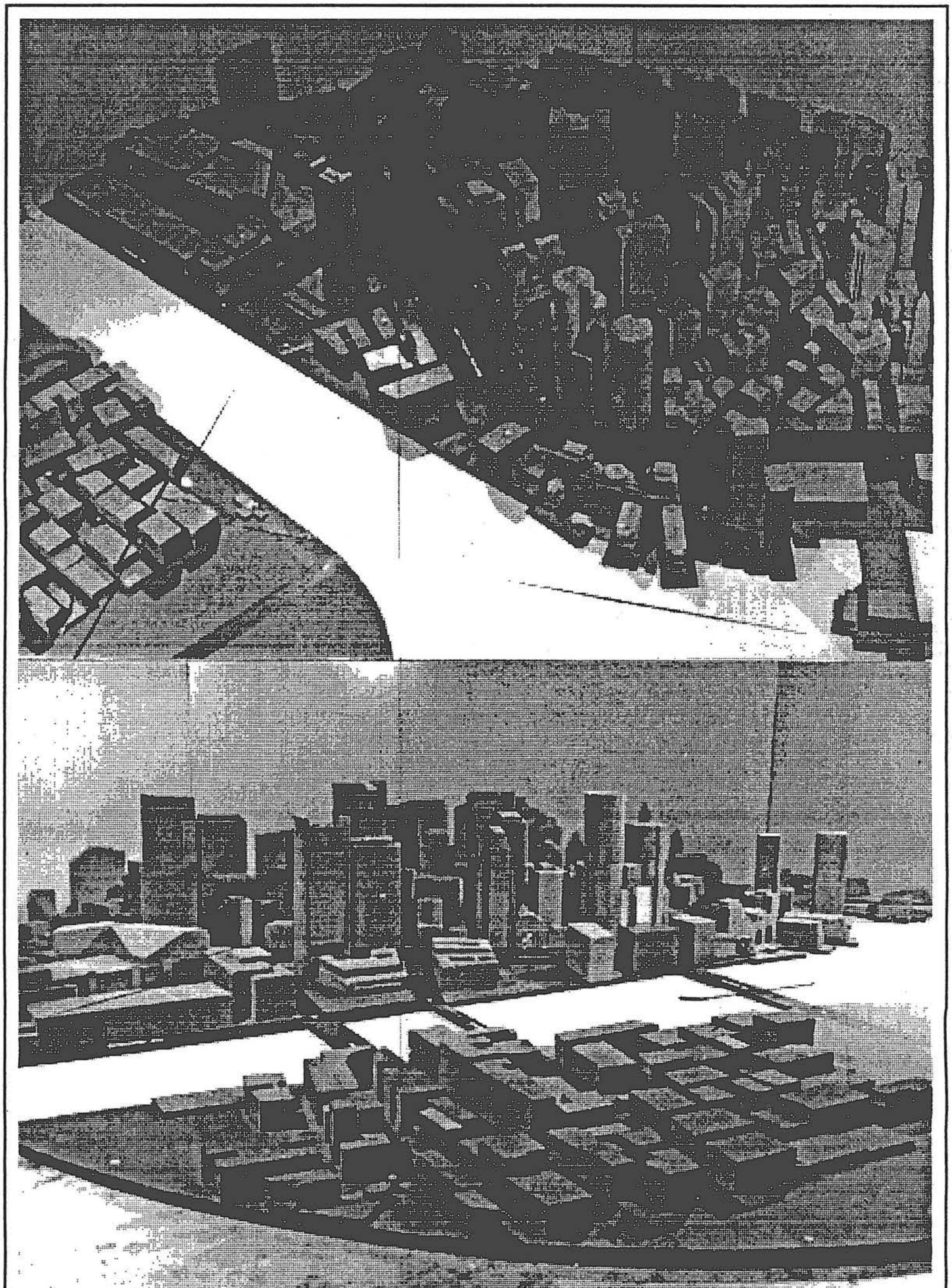

Figure 3 Boston-Edison Model Site Picture

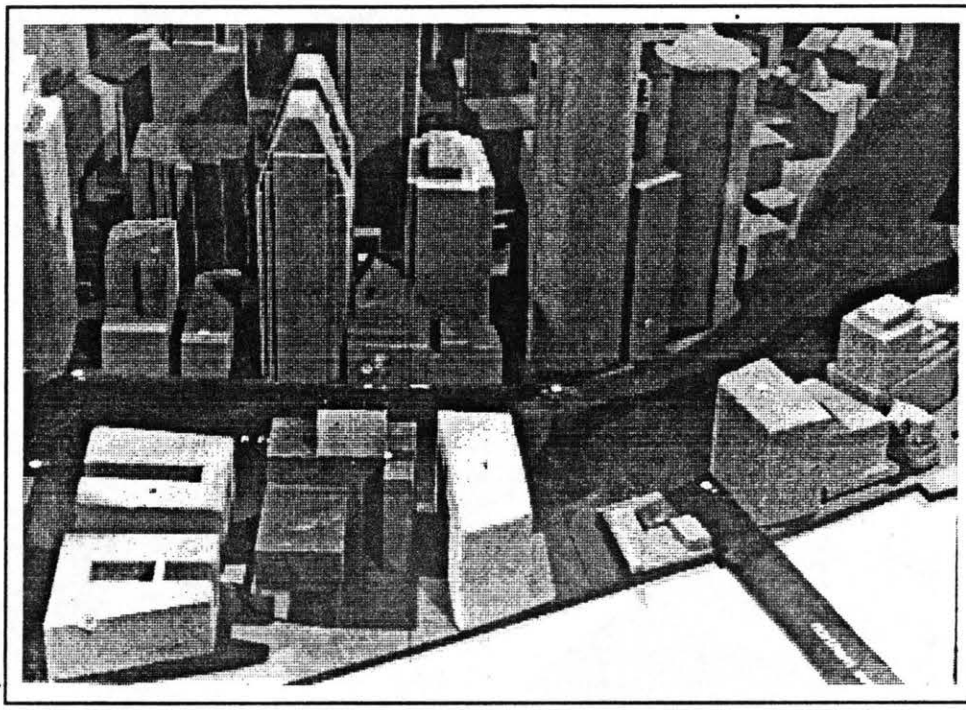

Figure 4 Boston-Edison Vent Building, Configuration 2B with 240 foot high stacks

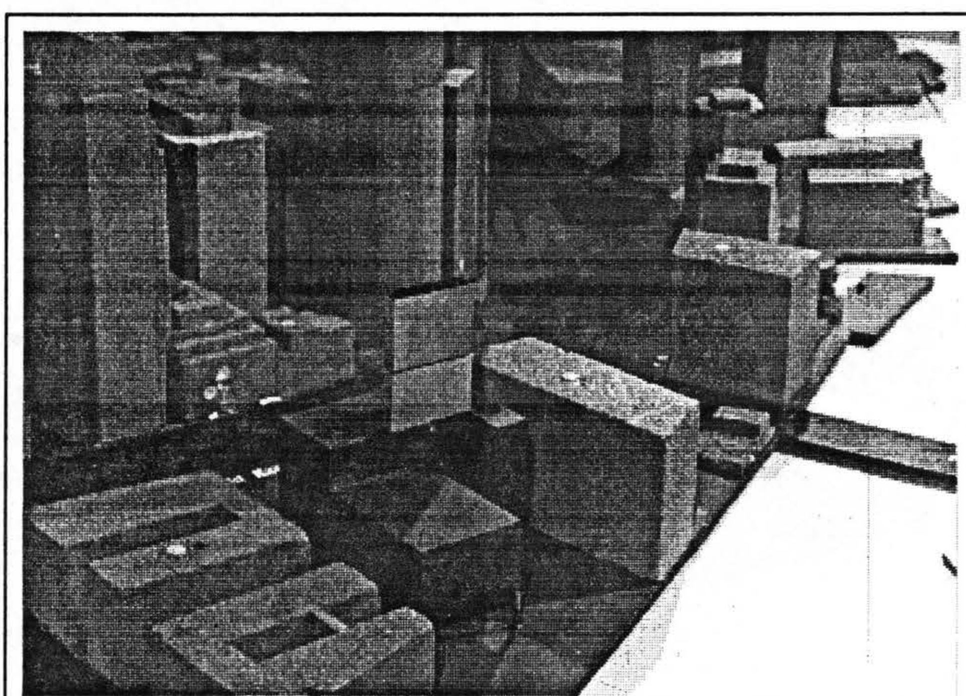

Figure 5 Boston-Edison Vent Building, Configuration 2B with 300 high stacks

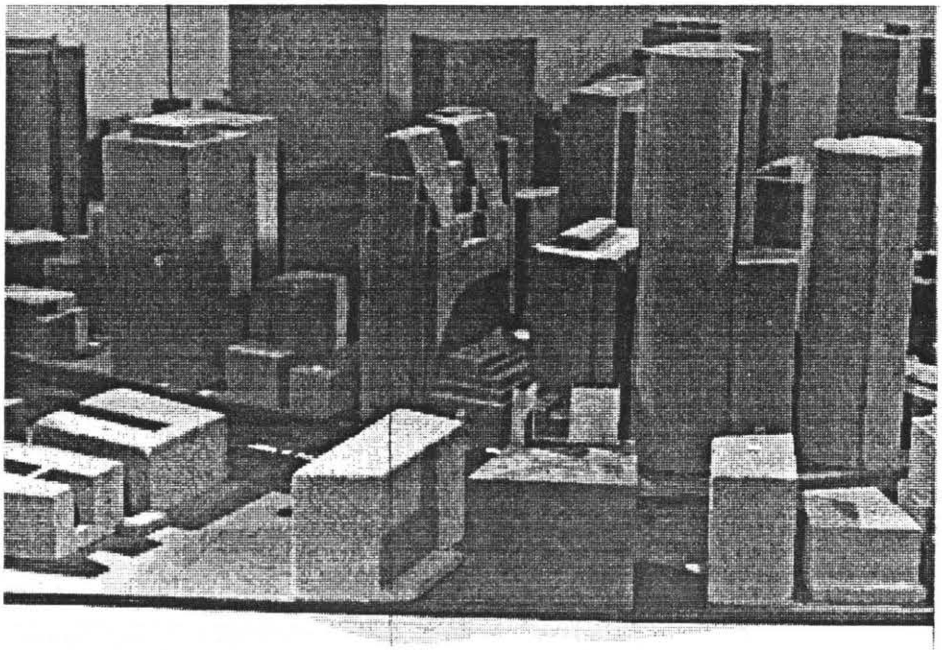

Figure 6 J. Hook Vent Building with 240 High Stacks

Figure 7 J. Hook Vent Building with 300 foot High Stacks

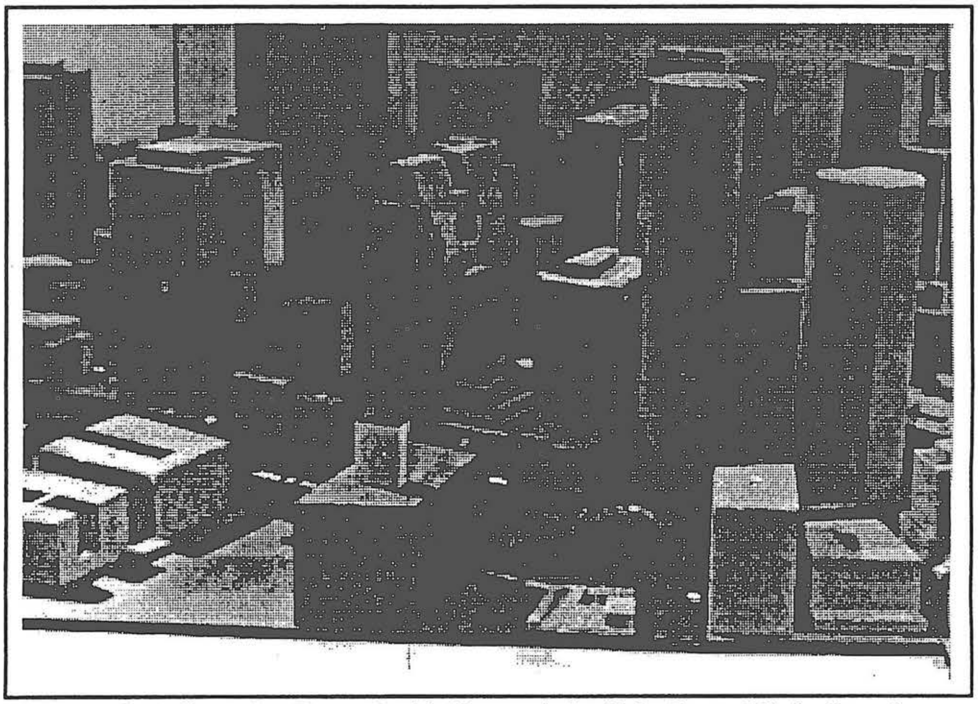

Figure 8 Atlantic Vent Building with 240 foot High Stacks

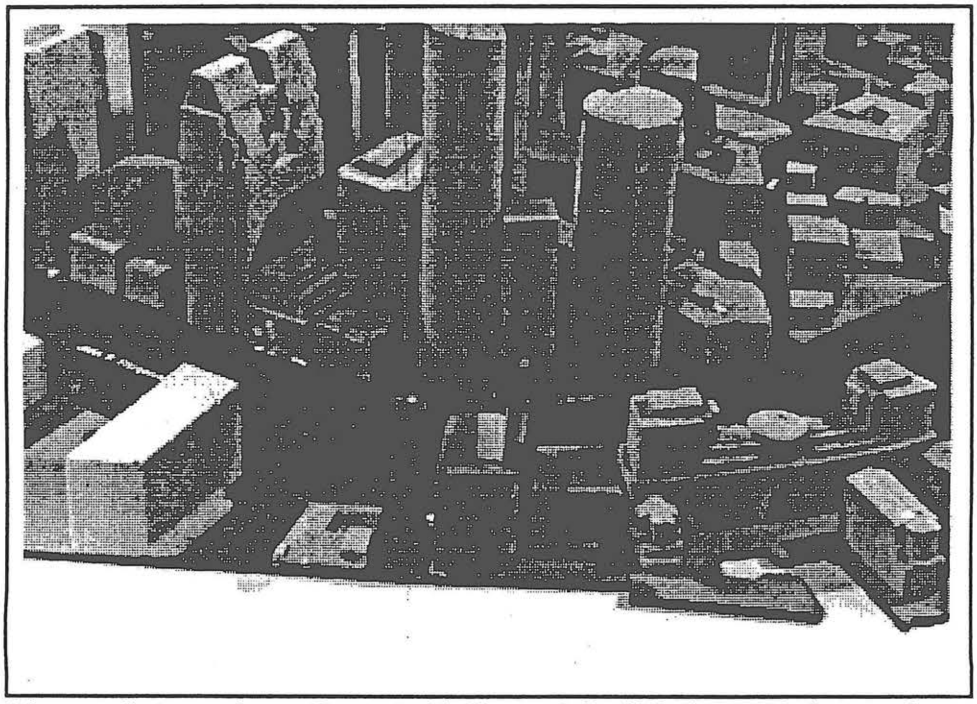

Figure 9 Appraiser Vent Building with 240 foot High Stacks

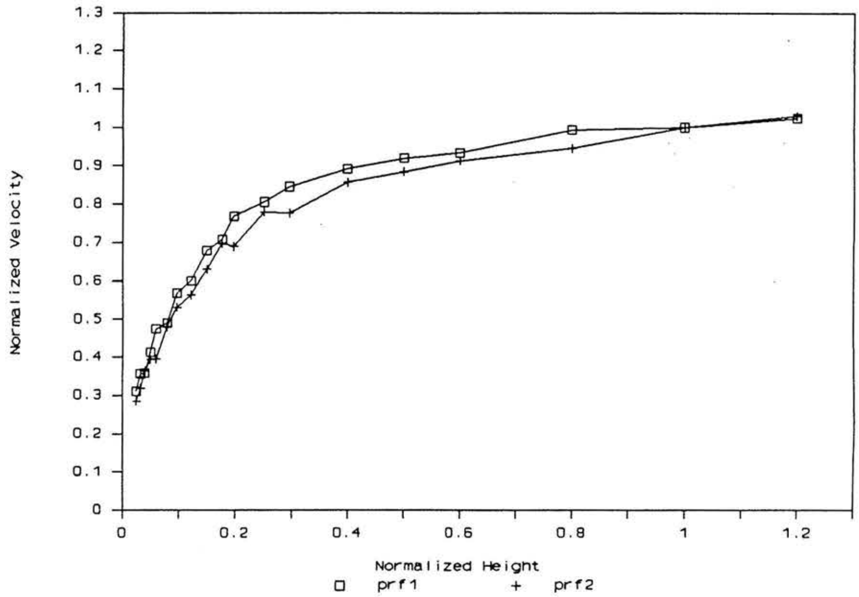

Figure 10 Mean Velocity Profiles for Profiles 1 and 2

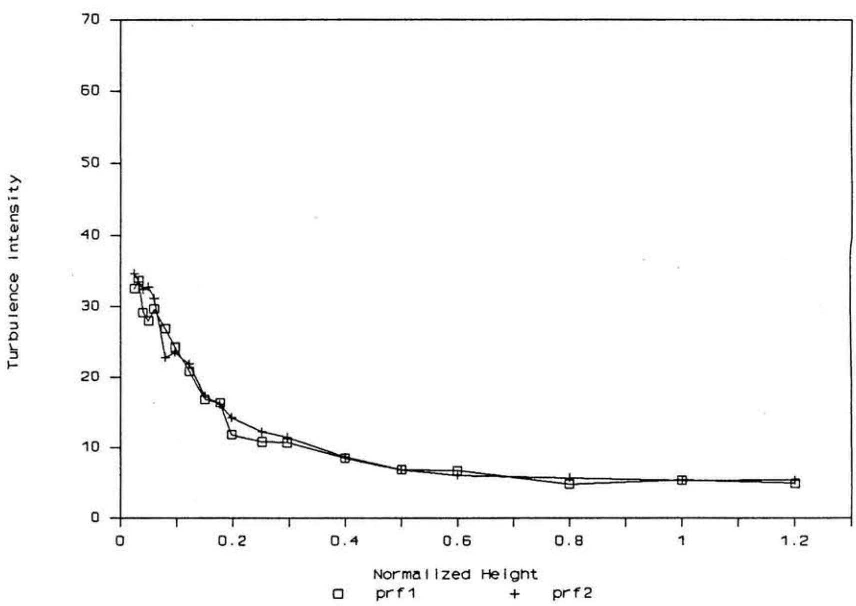

Figure 11 Turbulent Intensity Profiles for Profiles 1 and 2

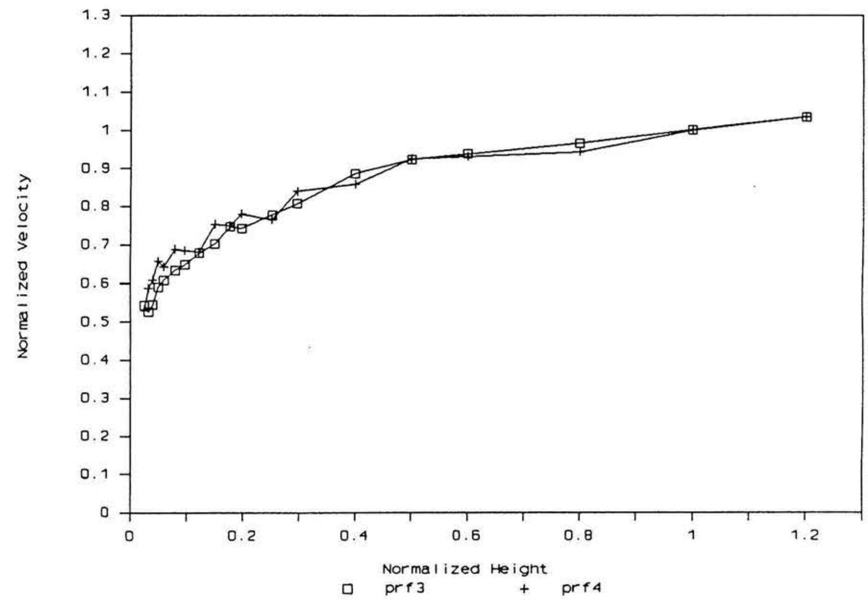

Figure 12 Mean Velocity Profiles for Profiles 3 and 4

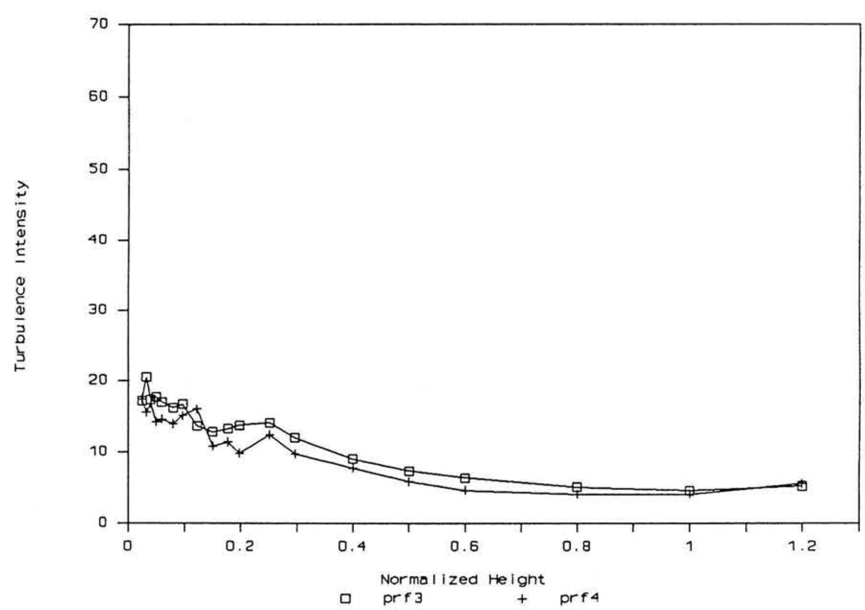

Figure 13 Turbulent Intensity Profiles for Profiles 3 and 4

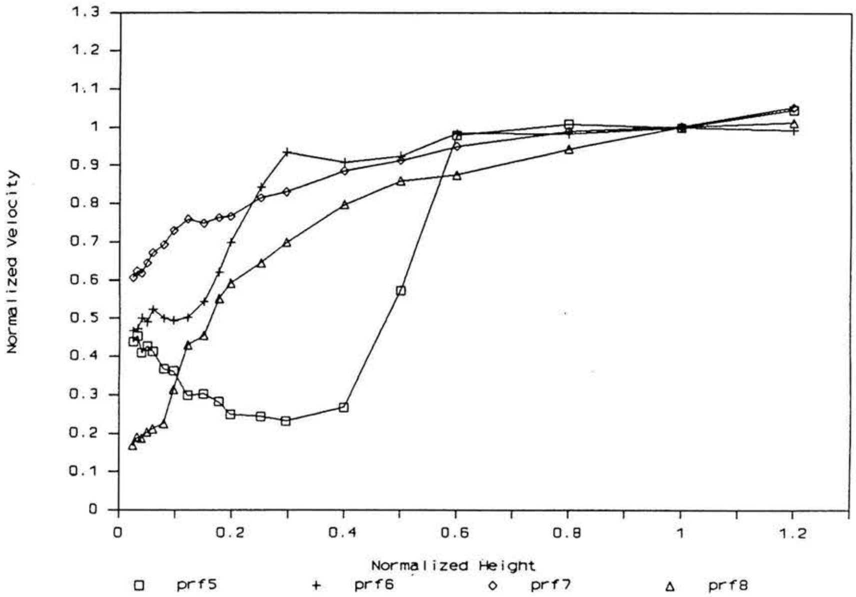

Figure 14 Mean Velocity Profiles for Profiles 5, 6, 7 and 8

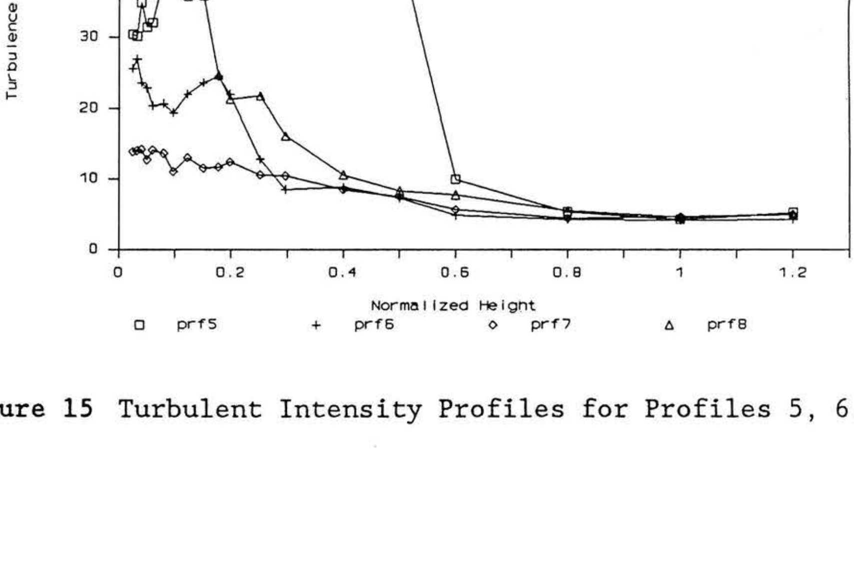

Figure 15 Turbulent Intensity Profiles for Profiles 5, 6, 7 and 8

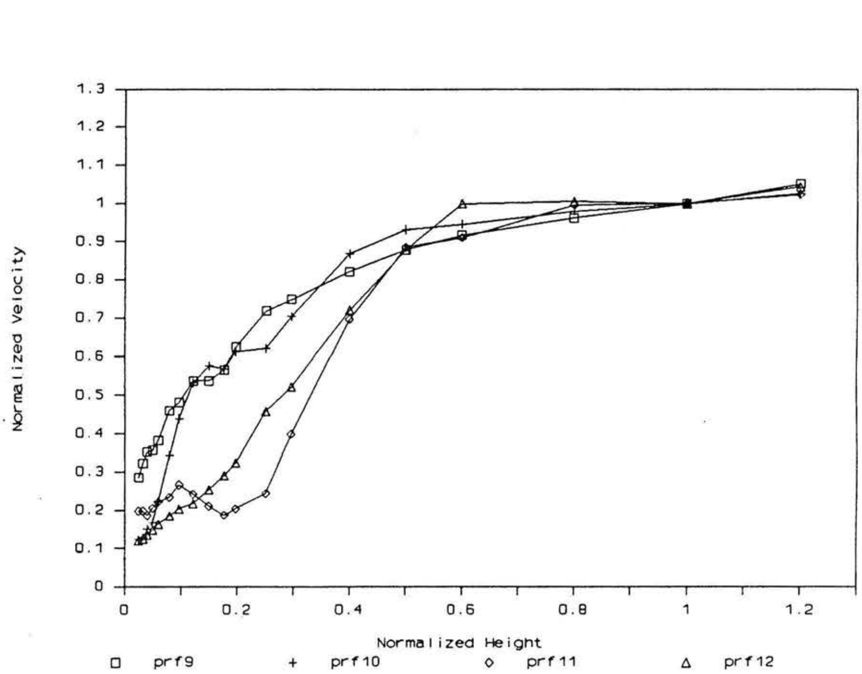

Figure 16 Mean Velocity Profiles for Profiles 9, 10, 11 and 12

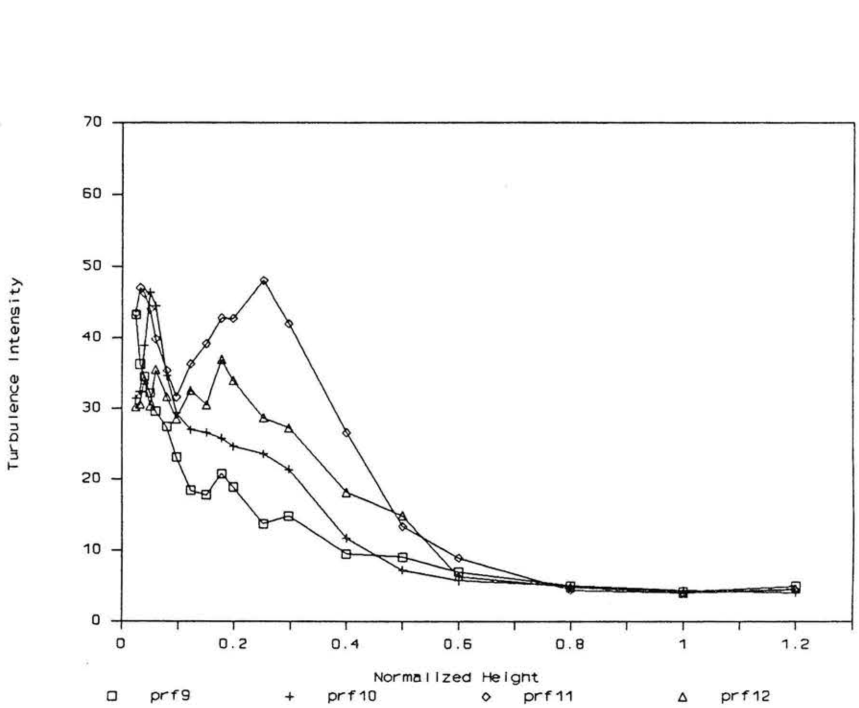

Figure 17 Turbulent Intensity Profiles for Profiles 9, 10, 11 and 12

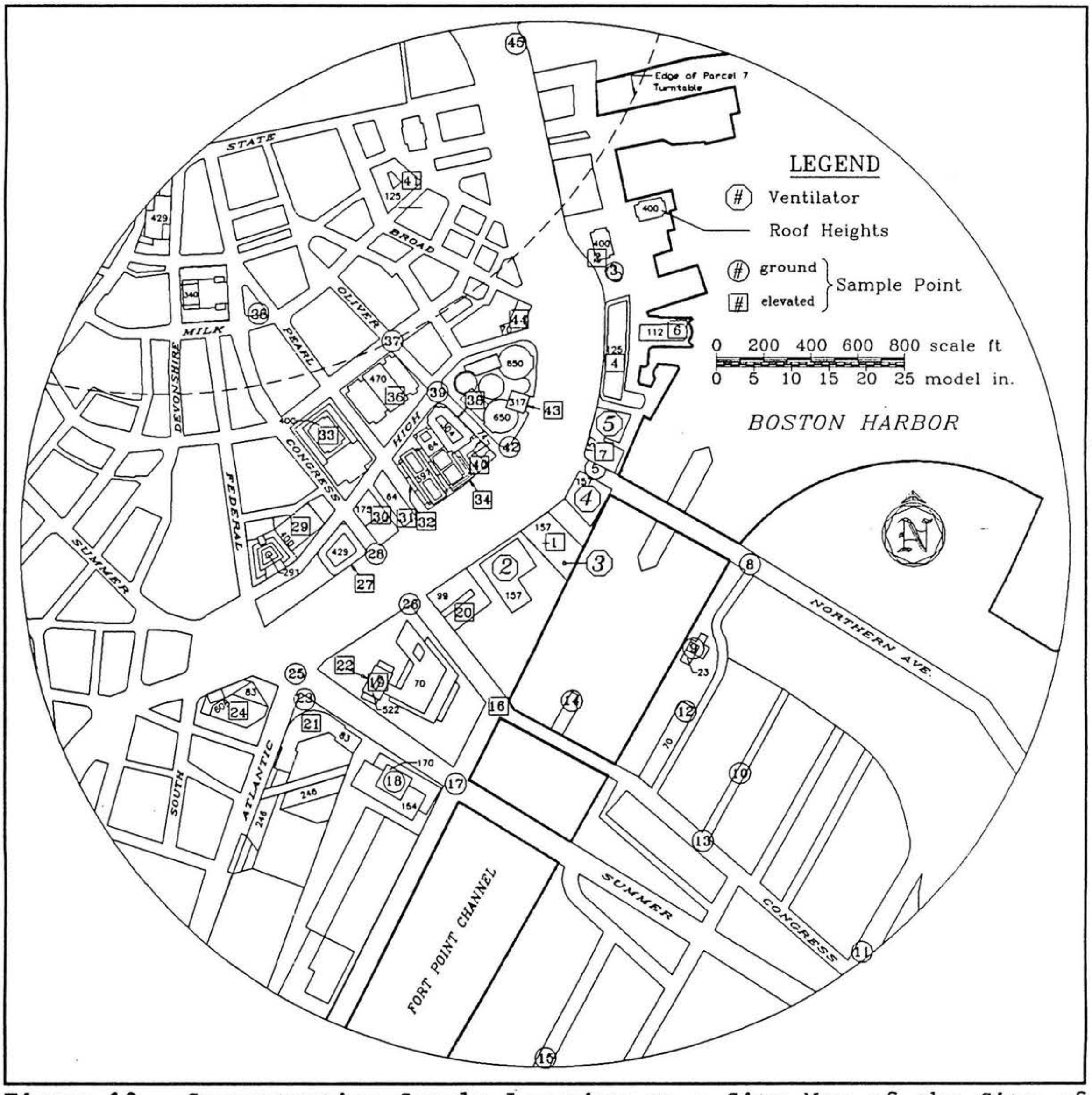

Figure 18 Concentration Sample Location on a Site Map of the City of Boston

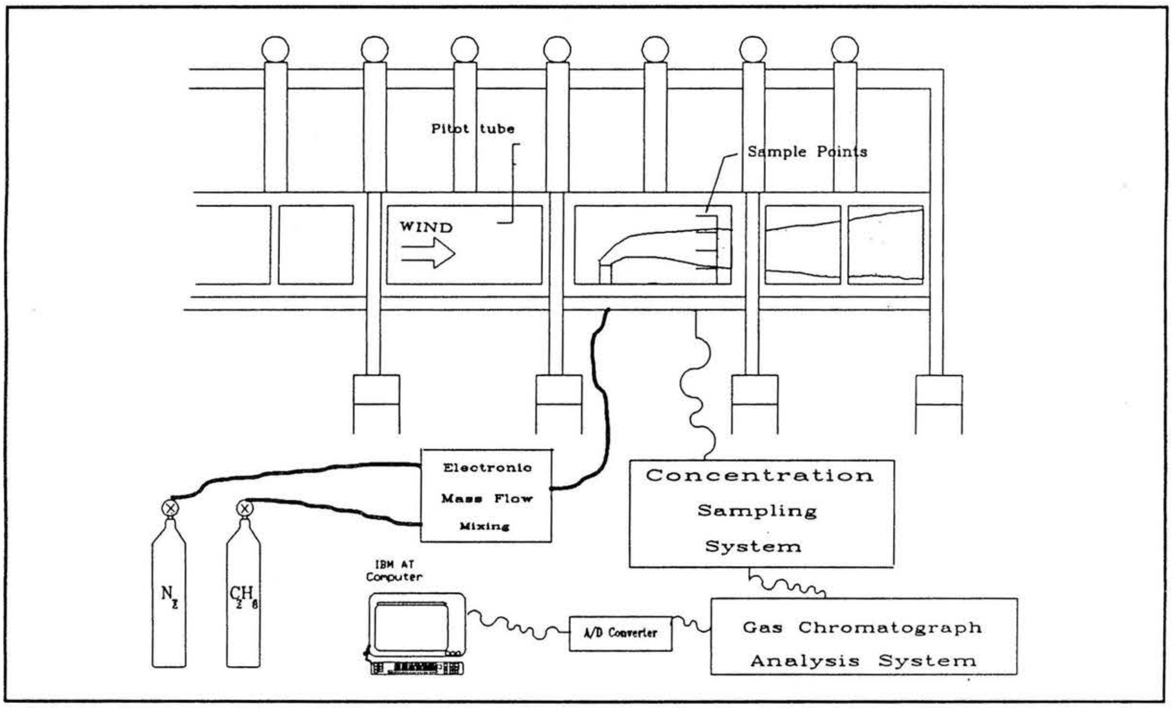

Figure 19 Wind Tunnel Gas Release and Sampling Schematic

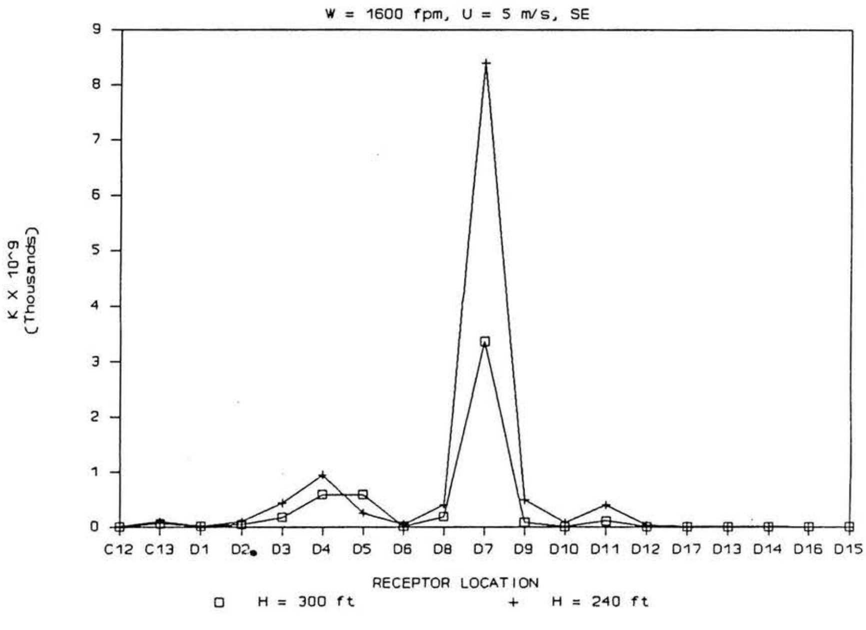

Figure 20 Influence of stack height on sampler concentrations

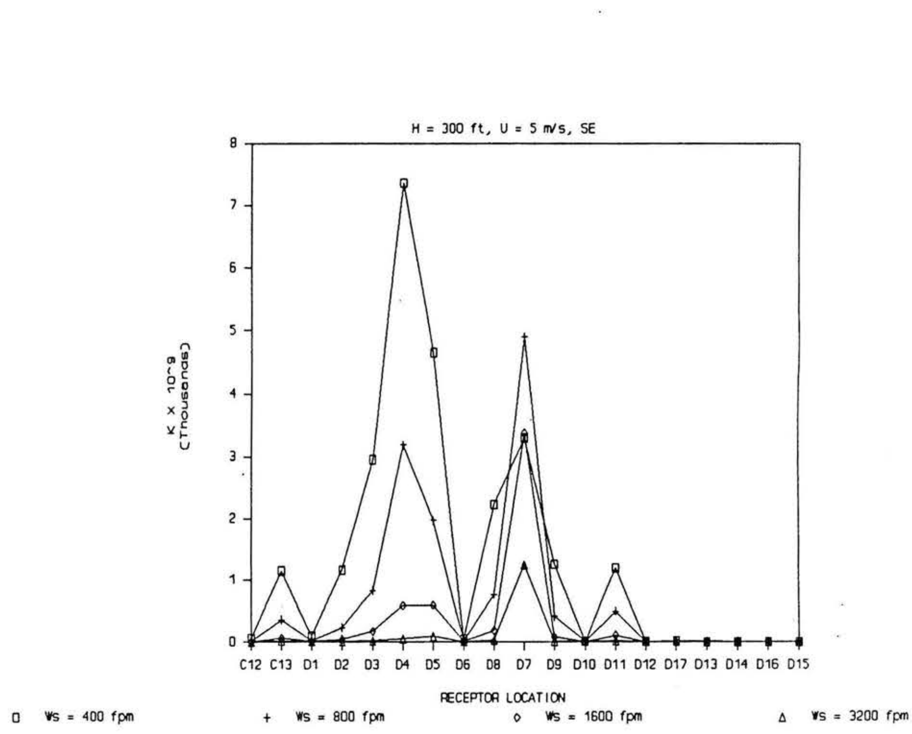

Figure 21 Influence of stack exhaust velocity on sampler concentrations

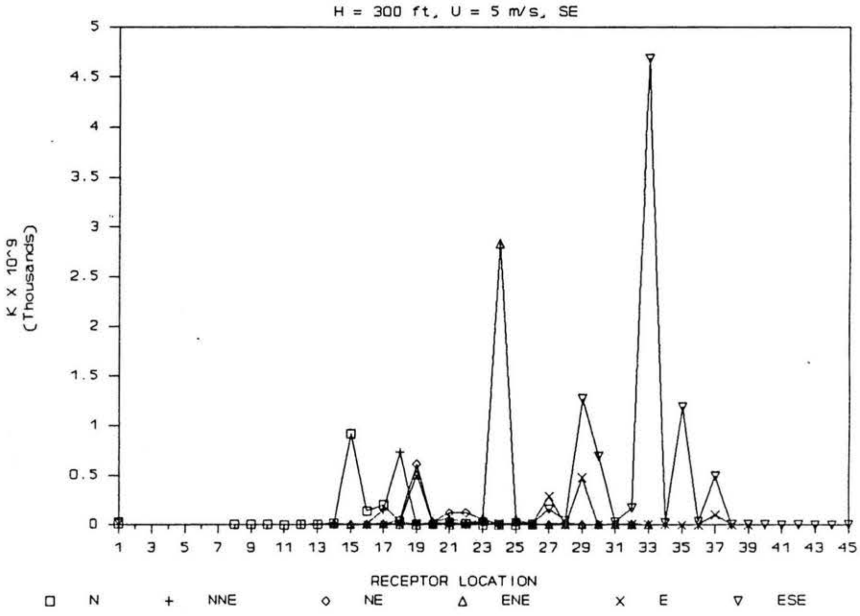

Figure 22 Influence of wind direction on sampler concentrations, N through ESE

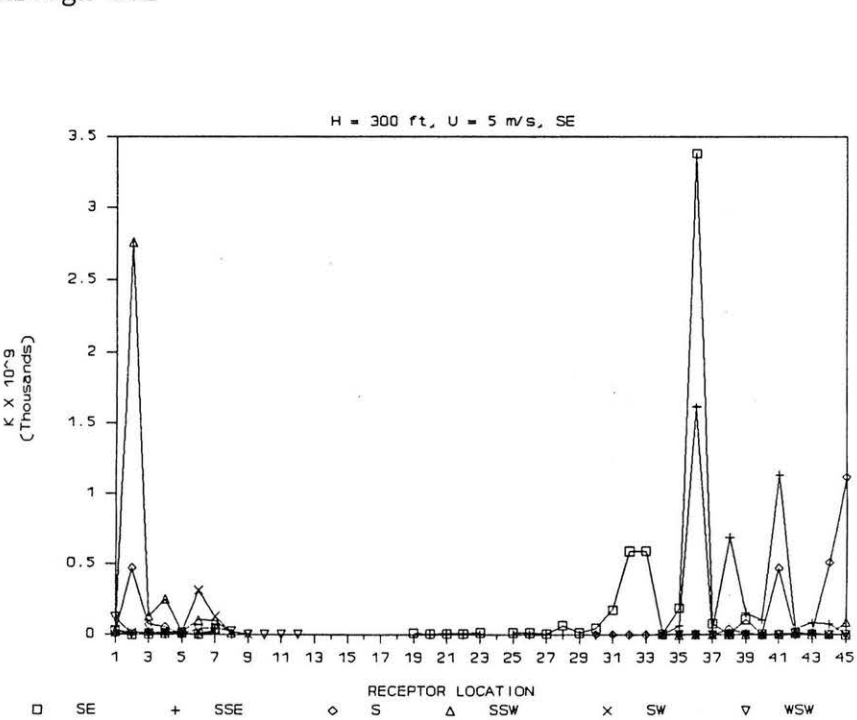

Figure 23 Influence of wind direction on sampler concentrations, SE through WSW

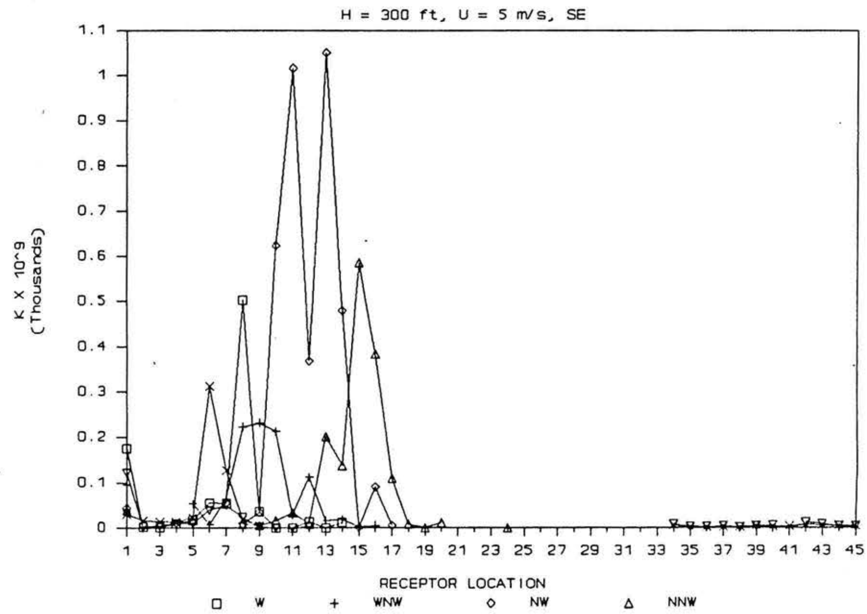

Figure 24 Influence of wind direction on sampler concentrations, W through NNW